Synthesis and characterization of $BaTiO_3$ Prepared by Molten Salt Synthesis Method

A

THESIS SUBMITTED IN PARTIAL FULFILLMENT

OF THE REQUIREMENTS FOR THE DEGREE OF

MASTER OF TECHNOLOGY

in

CERAMIC ENGINEERING

By

Ganesh Kumar Sahoo

Department of Ceramic Engineering

National Institute of Technology

Rourkela – 769 008

Synthesis and characterization of $BaTiO_3$ Prepared by Molten Salt Synthesis Method

A
THESIS SUBMITTED IN PARTIAL FULFILLMENT

OF THE REQUIREMENTS FOR THE DEGREE OF

MASTER OF TECHNOLOGY

in

CERAMIC ENGINEERING

By

Ganesh Kumar Sahoo

Under the Guidance of

Prof. Ranabrata Mazumder

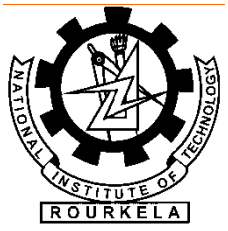

Department of Ceramic Engineering

National Institute of Technology

Rourkela – 769 008

DEPARTMENT OF CERAMIC ENGINEERING

NATIONAL INSTITUTE OF TECHNOLOGY,

ROURKELA-769008

CERTIFICATE

This is to certify that the thesis on "**Synthesis and characterization of $BaTiO_3$ Prepared by Molten Salt Synthesis Method**" submitted by **Mr. Ganesh Kumar Sahoo,** to the National Institute of Technology, Rourkela in partial fulfillment of the requirements for the award of the degree of **Master of Technology in Ceramic Engineering** is a record of bonafide research work carried out by him under my supervision and guidance. His thesis, in my opinion, is worthy of consideration for the award of degree of Master of Technology in accordance with the regulations of the institute.

The results embodied in this thesis have not been submitted to any other university or institute for the award of a Degree.

Prof. Ranabrata Mazumder

Department of Ceramic Engineering

National Institute of Technology

Rourkela

Acknowledgement

It is with a feeling of great pleasure that I would like to express my most sincere heartfelt gratitude to **Prof. Ranabrata Mazumder,** Dept. of Ceramic Engineering, NIT, and Rourkela for suggesting the topic for my thesis report and for his ready and able guidance throughout the course of my preparing the report. I thank you Sir for your help, inspiration and blessings.

I express my sincere thanks to **Prof. S. Bhattacharyya**, Head of the Department of Ceramic Engineering, NIT, Rourkela for providing me the necessary facilities in the department.

I would also take this opportunity to express my gratitude and sincere thanks to my honorable teachers **Prof. S.K. Pratihar Prof. J. Bera, Prof. B.Nayak, Prof. S.K.Pal** and **Mr.A.Chowdhury** for their invaluable advice, constant help, encouragement, inspiration and blessings.

Submitting this thesis would have been a Herculean job, without the constant help, encouragement, support and suggestions from my friends, especially **Sunil bhai ,Rashmi bhai ,Shyama, Ganga, Sanjay, Niroj and Smruti rekha** for their time to help. Although it will be difficult to record my appreciation to each and every one of them in this small space; I will feel guilty if I miss the opportunity to thank, **R.P Rana, Y. Nayak, J.P.Nayak, S.K.Rout, B.S.Sahu, S.Mohanty, H.Patra, A.Chakraborti** and others. I will relish your memories for years to come.

I would like to thank my parents and other family members, brother for their support for choices in all my life and their love, which has been a constant source of strength for everything I do.

I would also express my sincere thanks to laboratory Members of Department of Ceramic Engineering, N.I.T. Rourkela.

GANESH KUMAR SAHOO

Abstract

$BaTiO_3$ with a high permittivity is essential to enhance the volumetric efficiency of multi-layer ceramic capacitors (MLCCs) and depressed Curie peak is necessary for temperature stability. Recently, with the miniaturization of electronic devices, the downsizing of MLCC has been developed and accelerated. As a result, it is expected that the thickness of dielectric layers in MLCC soon will become less than 500 nm. Consequently, the particle size of the required $BaTiO_3$ raw materials will decrease from a few hundred nanometers to a few tens of a nanometer. Several processes have been carried out for the synthesis of nanosized $BaTiO_3$ but all of these methods are based on solution processes, they yield relatively small quantities of the desired nanostructures, and furthermore, in most cases, extremely toxic and unstable organometallic precursors are employed. Recently, molten salt synthesis method getting popularized for synthesis of large scale nanosized perovskite powder. In the current work emphasis has been given on low temperature synthesis of nanosized $BaTiO_3$ in large scale using molten salt method and their characterization. Three different eutectic salt mixtures have been tried namely NaOH-KOH, NaCl-KCl, LiCl-KCl. The study first optimized the different processing parameters e.g. salt systems, heat treatment temperature, holding time. By NaOH-KOH based salt system phase pure powder can be prepared at 175^oC. NaCl-KCl based system produced phase pure powder at 700^oC. LiCl-KCl based system failed to produce phase pure $BaTiO_3$ powder. Crystallite size of the synthesized powder found to be varying 30-43 nm depending on the processing time and temperature. TEM analysis revealed that particle size in the range of 70-100 nm. It has been observed that NaOH-KOH system synthesized powder can be densified (98%) at a temperature 1225^oC. Interestingly ultrafine grain size (200-500 nm) retained in highly dense sintered sample. In case of NaCl-KCl based powder only 91% density achieved, microstructure shows significant amount of porosity. Dielectric constant and loss factor of the sintered samples (ε_r =1400 and tanδ = 2% at 1 kHz) are on a par with $BaTiO_3$ prepared via conventional sintered sample. NaOH-KOH salt based prepared sample showed almost flatten Curie peak and NaCl-KCl salt system prepared sample showed broad Curie peak with a Curie temperature of 115^oC. The peak shift and broadening can be explained qualitatively from temperature dependence of volume fraction between surface cubic layer, bulk tetragonal layer, and gradient-lattice-strain layer (GLSL).

List of Figures		
		Page no.
Fig. 1.1	Interrelationship of piezoelectric and subgroups on the basis of symmetry	2
Fig. 1.2	Idealized permittivity of a ferroelectric material as a function of temperature	4
Fig.1.3	Hysteresis loops for ferroelectric materials	5
Fig. 1.4	"Hysteresis" for a lossy capacitor	6
Fig 1.5	Polarization vs. Electric field hysteresis curve in antiferroelectric materials.	9
Fig.1.6	Hysteresis loop for a shear plate of a ferroelectric $Pb(Zr,Ti)O_3$	9
Fig.1.7	Perovskite ABO_3 unit cell for $BaTiO_3$	11
Fig.1.8	Phase diagram of $BaTiO_3$	12
Fig.1.9	Dielectric constants of $BaTiO_3$ as a function of temperature	13
Fig.1.10	Crystal structure of $Bi_4Ti_3O_{12}$	16
Fig.2.1	Schematic illustration of the main processing stages in the MS method	27
Fig 4.1	The systematic Phase diagram of various salt (a) NaOH-KOH (b) NaCl-KCl (c) KCl-LiCl system.	39
Fig 4.1	The process for the preparation of $BaTiO_3$ powders by molten salt route	40
Fig 5.1	XRD pattern of $BaTiO_3$ Powder calcined at different temperature for 2h.	45
Fig 5.2	The average crystallite size of $BaTiO_3$ Powder calcined at different for 2h.	45

Contents

Chapter1

INTRODUCTION

1.1 Ferroelectricity

When an electric field is applied to an ideal *dielectric* material there is no long-range transport of charge but only a limited rearrangement of charge such that the dielectric acquires a dipole moment and is said to be polarized. Atomic polarization, which occurs in all materials, is a small displacement of the electrons in an atom relative to the nucleus. In ionic materials there is, in addition, ionic polarization involving the relative displacement of cation and anion sublattices. Dipolar materials, such as water, can become polarized because the applied electric field orients the molecules. Finally, space charge polarization involves a limited transport of charge carriers until they are stopped at a potential barrier, possibly a grain boundary or phase boundary.

An individual atom or ion in a dielectric is not subjected directly to an applied field but to a local field which has a very different value and under certain conditions, lattice polarization produces a local field which tends to stabilize the polarization further – a feedback mechanism. This points to the possibility of "*spontaneous polarization*" i.e., lattice polarization in the absence of an applied field. Such spontaneously polarized materials do exist and "ferroelectrics" constitute an important class among them [1]. The two conditions necessary in a material to classify it as a *ferroelectric* are (1) the existence of spontaneous polarization and (2) a demonstrated reorientation of the polarization by an applied electric field. Spontaneous polarization is defined as a stable polarization of a crystal in the absence of an external electric field.

The spontaneous polarization changes with temperature. There is a critical point—known as the *Curie temperature*—that defines the transition to a spontaneous polarization state from a state that is originally electrically neutral. Above the Curie temperature, the crystal is electrically neutral and its crystallographic phase is called paraelectric; below the Curie temperature, the crystal is spontaneously polarized and this crystallographic phase is called ferroelectric.

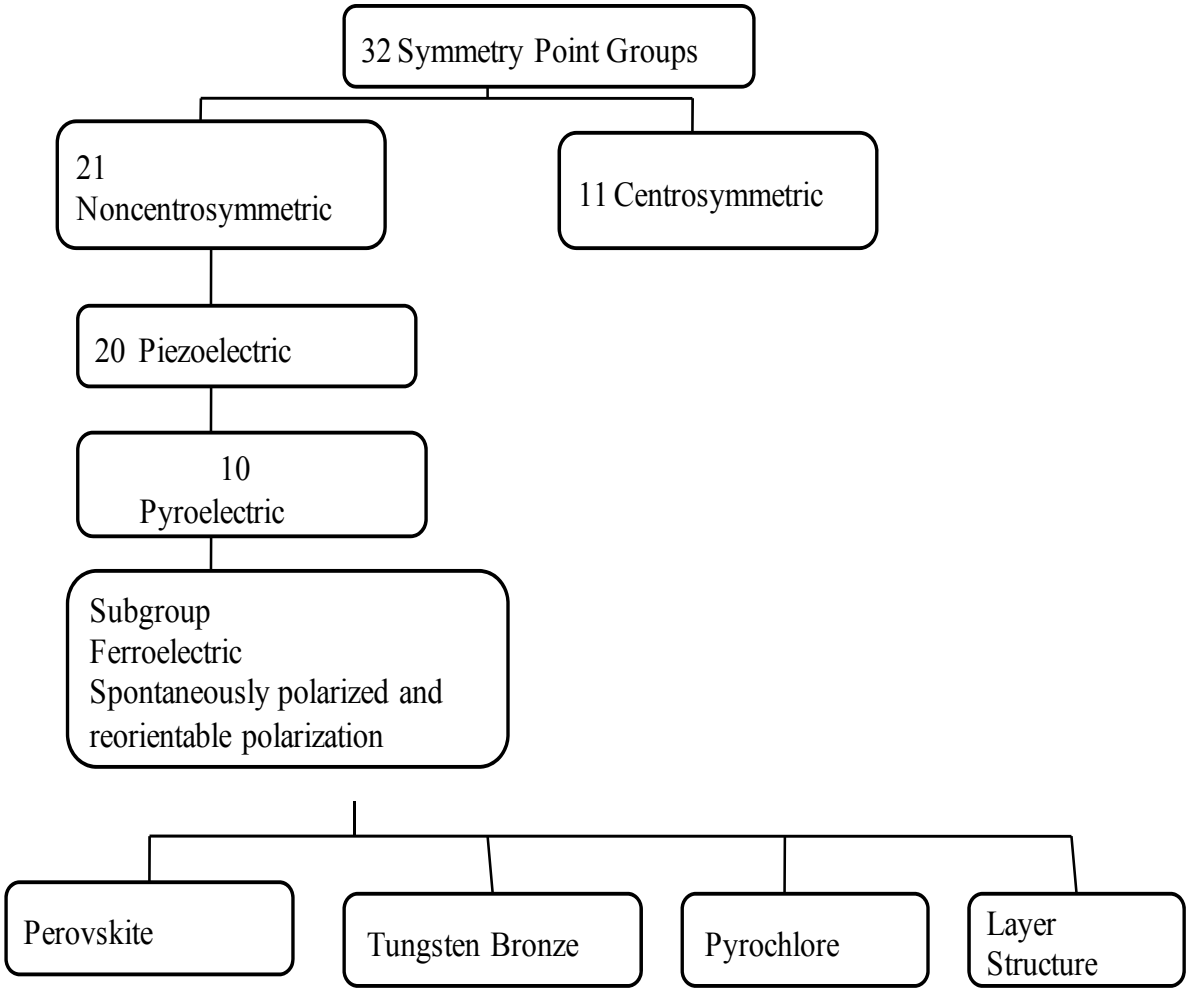

Fig.1.1 Interrelationship of piezoelectric and subgroups on the basis of symmetry.

Amongst the 32 point groups or classes of crystals, 21 classes are noncentrosymmetric and 20 of these are *piezoelectric* (discussed later). One class, although lacking a center of symmetry, is not piezoelectric because of other combined symmetry elements. Figure 1.1 shows that there are 10 crystal classes out of a possible 20 that are designated as *pyroelectric*. This group of materials possesses the unusual characteristic of being permanently polarized within a given temperature range. Unlike the more general piezoelectric classes that produce a polarization under stress, the pyroelectrics develop this polarization spontaneously and form permanent dipoles in the structure. This polarization also changes with temperature—hence, the term pyroelectricity. A subgroup of the spontaneously polarized pyroelectrics is a very special

category of materials known as ferroelectrics. Similar to pyroelectrics, materials in this group possess spontaneous polarization; however, unlike pyroelectrics, the direction of the spontaneous polarization is orientable by an electric field of some magnitude less than the dielectric breakdown of the material itself.

Below the curie temperature, ferroelectric crystals generally develop a random domain structure, leading to a net zero polarization of each crystal. Within each ferroelectric domain the polarization is in the same direction with a domain wall separating regions with different polarization directions. This structure is necessary to minimize free energy due to the development of anisotropic strains and depolarization fields below T_C. Domain walls are characterized by the angle between the polarization directions on either side of the wall. Thus a 180^o domain wall demarks a boundary between antiparallel domains, while a 90^o wall would be formed at the boundary between domains pointed "up" and "left", for example. The allowed angles for domain walls depend on the orientation of the spontaneous polarization allowed by symmetry. Thus in rhombohedrally distorted perovskites, there are no 90^o domain walls like a tetragonal perovskite, but instead 71^o and 109^o walls. A more complete picture of the way the polarization changes as a domain wall is crossed is given by Cao and Cross [12].

1.2 Curie Temperature and Hysteresis

At a particular temperature, nearly all ferroelectric materials pass through a ferroelectric to paraelectric phase transition (in several examples materials decompose prior to passing into the paraelectric state) [2]. The temperature at which a ferroelectric material reverts to the high temperature paraelectric phase is called the Curie temperature (T_C). On cooling through T_C into a ferroelectric phase, a reorientable spontaneous polarization is developed.

In ferroelectrics dominated by a displacive phase transition, such as perovskite materials, the temperature dependence of the permittivity varies for 1st and 2nd order phase transitions. Fig. 1.2 illustrates the temperature dependence of the permittivity for displacive ferroelectric materials exhibiting first or second order phase transitions. Second order phase transitions, which are common for rhombohedral compositions, are generally characterized by a broad peak in permittivity. Ferroelectrics undergoing first order phase transitions, typical of tetragonal

perovskite materials, however show a fairly flat permittivity with increasing temperature right up to the T_c.

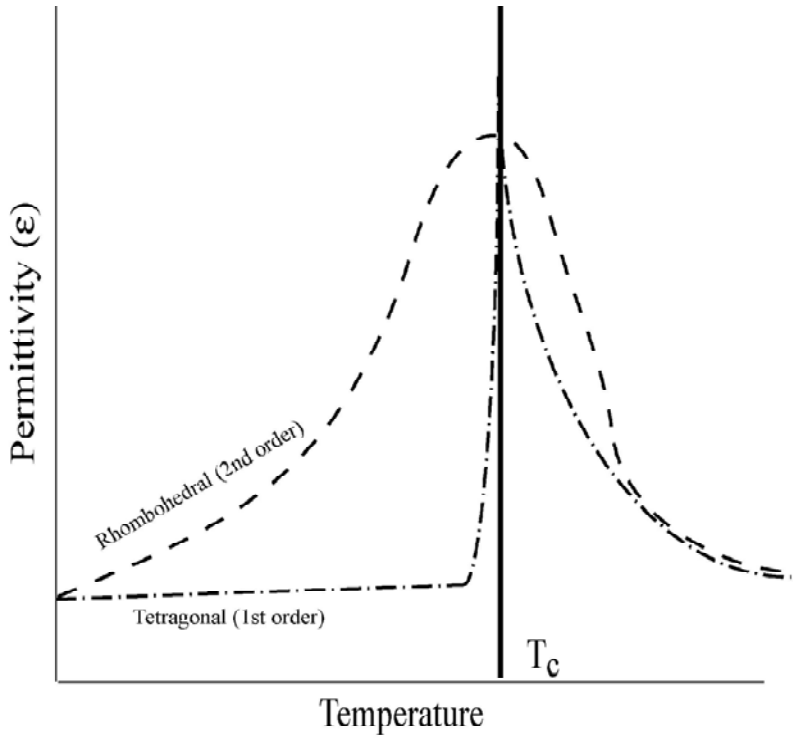

Fig 1.2 Idealized permittivity of a ferroelectric material as a function of temperature.

The reciprocal permittivity $1/\varepsilon$ is known to be linear with respect to the temperature in a wide range in the paraelectric phase (so-called Curie-Weiss law),

$$\varepsilon = \frac{C}{T - T_0} \qquad (1.1)$$

where C is the Curie-Weiss constant and T_0 the Curie-Weiss temperature. T_0 is slightly lower than the exact transition temperature T_c. For displacive transitions (e.g., $BaTiO_3$, $PbTiO_3$, $KNbO_3$), the Curie Constant is very high (~ 10^4 – 10^5 K) and the paraelectric phase is microscopically nonpolar. For order-disorder transition (e.g., TGS, KH_2PO_4), the Curie Constant

is of the order of T_0 and the paraelectric phase is nonpolar on macroscopic or thermally averaged sense.

The commonly accepted criterion of ferroelectricity is a *hysteresis loop* on a polarization (P) - electric field (E) display. For non-ferroelectric samples, a straight line results; while for a ferroelectric sample, a hysteresis loop is generated. The hysteresis (Fig.1.3) arises from the energy needed to reverse the metastable dipoles during each excursion of the field. The area of the loop represents energy that is dissipated within the sample as heat. Under ideal conditions and in a single-crystal, the whole domain-wall structure is wiped out by the field at point D and new domains with orientation opposite to those of P_R (remanent polarization) start nucleating at the sample surface once the field reverses direction. The mechanisms of domain nucleation and propagation depend on many factors and even on the form of the material [3] (bulk or thin-film form). For ceramics, a somewhat higher coercive field may be found. This represents a distribution of values for individual grains, each of which is constrained by its neighbours. The loops for ceramics are much more "slanted" than those of single crystals which are square in shape.

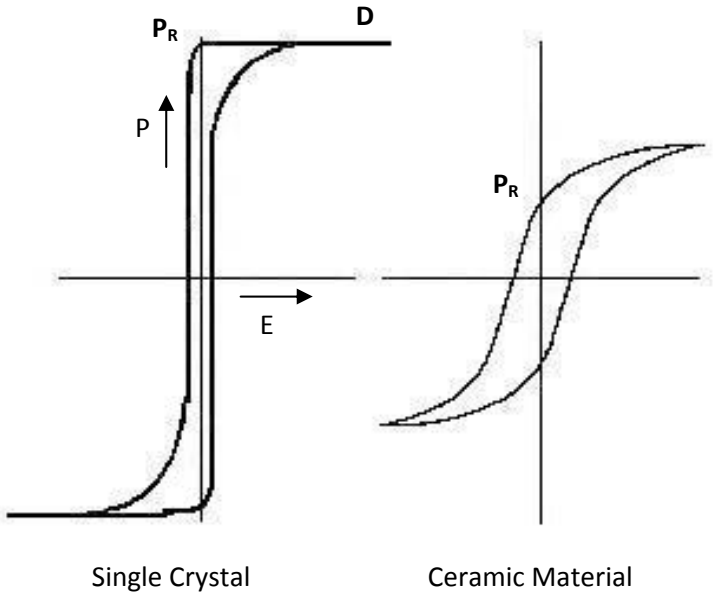

Fig 1.3 Hysteresis loops for ferroelectric materials

Many ceramics are, however, not good insulators, they conduct to some degree. The vertical deflection is then partly caused by dielectric displacement and partly by conduction. This conduction is either linear, that is, proportional to the field, or nonlinear, increasing as some

power of the field. If we have a linear dielectric with linear conduction, the straight line figure changes to an ellipse. The resultant P-E loop of Fig. 1.4 shows phase shift, and we speak of it as a lossy linear capacitor.

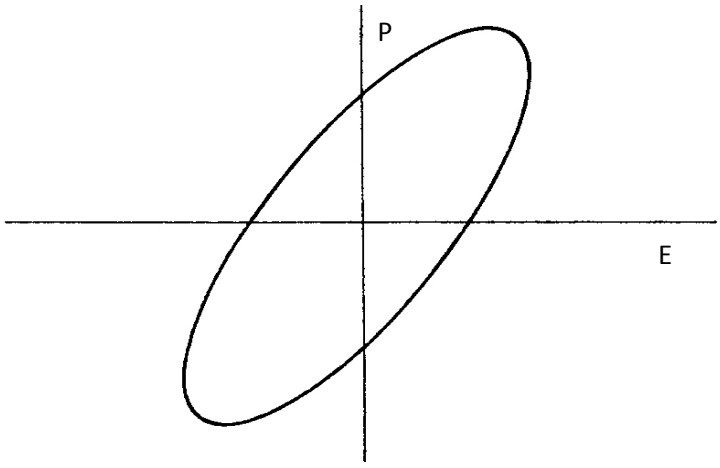

Fig. 1.4 "Hysteresis" for a lossy capacitor

Hence, not all solids with electrical hysteresis are ferroelectric. A saturating hysteresis loop is a very good evidence of true ferroelectricity.

1.3 Different origins of ferroelectricity

Recently, Mostovoy et.al. [4] classified ferroelectrics into two different classes, viz., 1) proper ferroelectrics and 2) improper ferroelectrics, and the detailed classification is given in Table 1.1.

Table 1.1: Classification of ferroelectrics

	(Mechanism of inversion symmetry breaking)	Materials
Proper	Covalent bonding between $3d^0$ transition metal (Ti) and oxygen	$BaTiO_3$, PZT
	Polarization of $6s^2$ lone pair of Bi or Pb	$BiMnO_3$, $BiFeO_3$, $Pb(Fe_{2/3}W_{1/3})O_3$
Improper	Structural transition 'Geometric ferroelectrics'	K_2SeO_4, Cs_2CdI_4 hexagonal $RMnO_3$
	Charge ordering 'Electronic ferroelectrics'	$LuFe_2O_4$
	Magnetic ordering 'Magnetic ferroelectrics'	Orthorhombic $RMnO_3$, RMn_2O_5, $CoCr_2O_4$

Perovskites consist of corner-sharing O_6 octahedra with a transition metal ion in the centre. Almost all the ferroelectric perovskites contain non-magnetic transition metal ions with an empty *d*-shell (d^0 configuration), for example Ti^{4+}, Nb^{5+} and W^{6+}. These positively charged ions like to form 'molecules' with one (or several) of the neighbouring negative oxygen ions. In all of these systems ferroelectricity originates from a shift of the transition metal ion from the centre of the O_6 octahedron. In this way a stronger covalent bond with one (or three) instead of six weaker bonds with neighbouring oxygen atoms is formed [5]. This collective shift of cations and anions inside a periodic crystal induces a bulk electric polarization. The mechanism of the covalent bonding (electronic pairing) in such molecules is the virtual hopping of electrons from the filled oxygen shell to the empty *d* shell of a transition metal ion.

Some compounds, such as $BiMnO_3$ or $BiFeO_3$ with magnetic Mn^{3+} and Fe^{3+} ions, are ferroelectric. Here, however, it is the Bi ion with two electrons on the 6*s* orbital (lone pair) that moves away from the centrosymmetric position in its oxygen surrounding [6].

If, on the other hand, polarization is only a part of a more complex lattice distortion or if it appears as an accidental by-product of some other ordering, the ferroelectricity is called 'improper' [7]. For example, the hexagonal manganites $RMnO_3$ (R = Ho–Lu, Y) show a lattice transition which enlarges their unit cell. An electric dipole moment, appearing below this transition, is induced by a nonlinear coupling to nonpolar lattice distortions, such as the buckling of R–O planes and tilts of manganese–oxygen bipyramids (geometric ferroelectricity) [8].

1.4 Antiferroelectric Materials

Materials with sublattices containing compensating dipoles are called antiferroelectric. These materials are characterized by a phase transition from a state of lower symmetry (generally low temperature phase) to that of a higher symmetry (high temperature phase). The low symmetry state can be regarded as a slightly distorted high symmetry state. In contrast to ferroelectric crystals, it has no permanent electric polarization, and the crystal lattice can be regarded as consisting of two interpenetrating sublattices with equal but opposite electric polarization (antipolarized state).

In the high symmetry phase, the sublattice are unpolarized and indistinguishable. In general, antiferroelectric crystal have more than one axis along which the sublattices can polarize. Therefore, the low symmetry phase consists of regions of homogeneous antipolarization which differ only in the orientation of the axis along which antipolarization has occurred. These regions are called antiferroelectric domains and can be observed by the polarizing microscope. Because these domains have no permanent electric dipole moment, an electric field generally has little influence on domain structure [9].

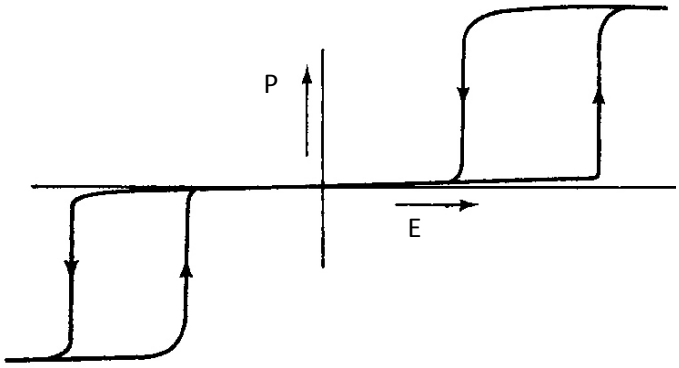

Fig.1.5 Polarization vs. Electric field hysteresis curve in antiferroelectric materials

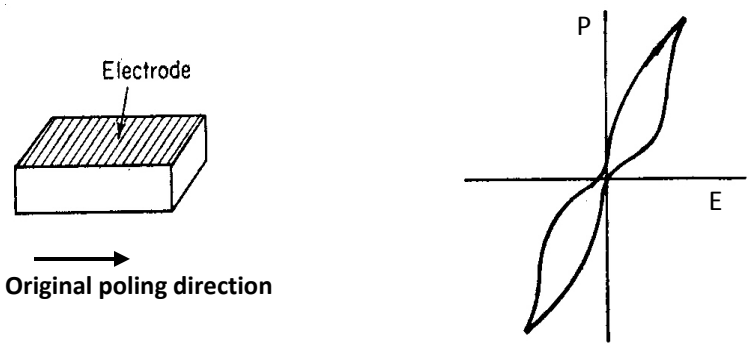

Fig.1.6 Hysteresis loop for a shear plate of a ferroelectric $Pb(Zr,Ti)O_3$

The dielectric constant of antiferroelectric crystals is generally larger than that of nonferroelectric crystal and has an anomalous temperature dependence. It increases as the transition temperature is approached and drops when antipolarization occurs.

Some antiferroelectrics undergo phase transition from an antipolarized state into a spontaneously polarized ferroelectric state under a sufficiently strong electric field applied along an antiferroelectric axis (Fig.1.5). The crystal reverts, however, to the antiferroelectric state when the electric field is removed. Compounds with antiferroelectric properties are $PbZrO_3$, $PbHfO_3$, $NaNbO_3$, WO_3, $NH_4H_2PO_4$. Merz [10] showed similar looking double loops for $BaTiO_3$ crystals

at a temperature just above the Curie point. The loops, in this case, show a parelectric (simple cubic) to ferroelectric (tetragonal) transition. Still another sort of double loop can be generated by exciting a "shear plate" of a normal poled ferroelectric and then re-electroded in an orthogonal direction. Fig.1. 6 shows such a loop for a Sr-modified $Pb(Zr,Ti)O_3$ sample of the configuration shown in the figure [9]. Hence, double loop is not necessarily a signature of the antiferroelectric state.

1.5 Some Important Ferroelectric Materials

Normally, ceramic ferroelectrics may be classified into four groups depending on their crystal structure: (1) the oxygen octahedral group (perovskite) (2) the tungsten–bronze group, (3) the pyrochlore group and (4) the bismuth layer–structure group. Of these, the ABO_3 perovskite type is by far the most important category, economically. The families of compositions, e.g., $BaTiO_3$, PZT (lead zirconate titanate), PLZT (lead lanthanum zirconate titanate), PT (lead titanate), PMN (lead magnesium niobate), and $(Na,K)NbO_3$ represent the bulk of the ferroelectric ceramics manufactured in the world today.

Most technologically important ferroelectrics are oxides with a perovskite structure. The great sensitivity of ferroelectrics to chemistry, defects, electrical boundary conditions and pressure arises from a delicate balance between the long range coulomb force (which favours the ferroelectric state) and short range repulsion (which favours the non-polar cubic structure) [11].

1.5.1 Barium titanate

$BaTiO_3$ is the first piezoelectric transducer ceramic ever developed. $BaTiO_3$ is isostructural with the mineral perovskite ($CaTiO_3$) and so is referred to as 'a perovskite'. Above its Curie point (approximately 130^oC) the unit cell is cubic. Below the Curie point the structure is slightly distorted to the tetragonal form with a dipole moment along c direction. Other transformations occur at temperatures close to 0^oC and -80^oC: below 0^oC the unit cell is orthorhombic with the polar axis parallel to a face diagonal and below -80^oC it is rhombohedral with the polar axis along a body diagonal.

A typical ABO_3 unit-cell structure is given in Fig.1.7 For example, the $BaTiO_3$ unit cell consists of a corner-linked network of oxygen octahedra with Ti^{4+} ions occupying sites (B sites)

within the octahedral cage and the Ba^{2+} ions situated in the interstices (A sites) created by the linked octrahedra. When an electric field is applied to this unit cell, the Ti^{4+} ion moves to a new position along the direction of the

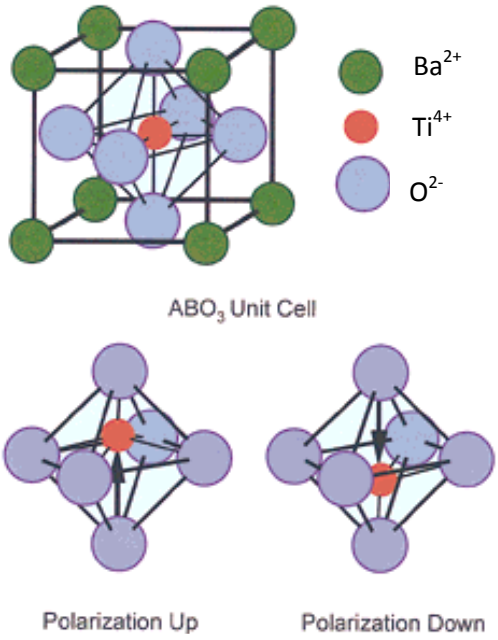

Fig.1.7 Perovskite ABO_3 unit cell for $BaTiO_3$ illustrating 180° polarization reversal for two of the six possible polarization states produced by displacement of the central cation in the tetragonal plane.

applied field. Because the crystallite and, hence, the unit cell is randomly oriented and the ions are constrained to move only along certain crystallographic directions of the unit cell, it is most often the case that an individual ionic movement only closely approximates an alignment with the electric field. However, when this ionic movement does occur, it leads to a macroscopic change in the dimensions of the unit cell and the ceramic as a whole. The dimensional change can be as large as a few tenths of a percent elongation in the direction of the field and approximately one-half of that amount in the other two orthogonal directions. The original random orientation of the domain polarization vectors (virgin condition) can be restored by heating the material above its T_c. This process is known as thermal depoling.

Also, as shown in Fig.1.7 the reversibility of the polarization is caused by the displacement of the central Ti^{4+} ion. The displacement is illustrated here as occurring along the **c** axis in a tetragonal structure, although it should be understood that it can also occur along the orthogonal **a** or **b** axes as well. The views of "polarization up" and "polarization down" (representing 180° polarization reversal) show two of the six possible permanent polarization positions.

Though $BaTiO_3$ is the first piezoelectric transducer ceramic ever developed, its use in recent years has shifted away from transducers to an almost exclusive use as high-dielectric constant capacitors of the discrete and multilayer (MLC) types. The reasons for this are primarily twofold: (1) its relatively low T_c of 130°C, which limits its use as high-power transducers, and (2) its low electromechanical coupling factor in comparison to PZT (0.52 vs 0.48), which limits its operational output.

$BaTiO_3$ assumes five different crystal structures namely, hexagonal, cubic, tetragonal, orthorhombic, and rhombohedral. The hexagonal and cubic structures are paraelectric while the tetragonal, orthorhombic and the rhombohedra forms are ferroelectric in nature

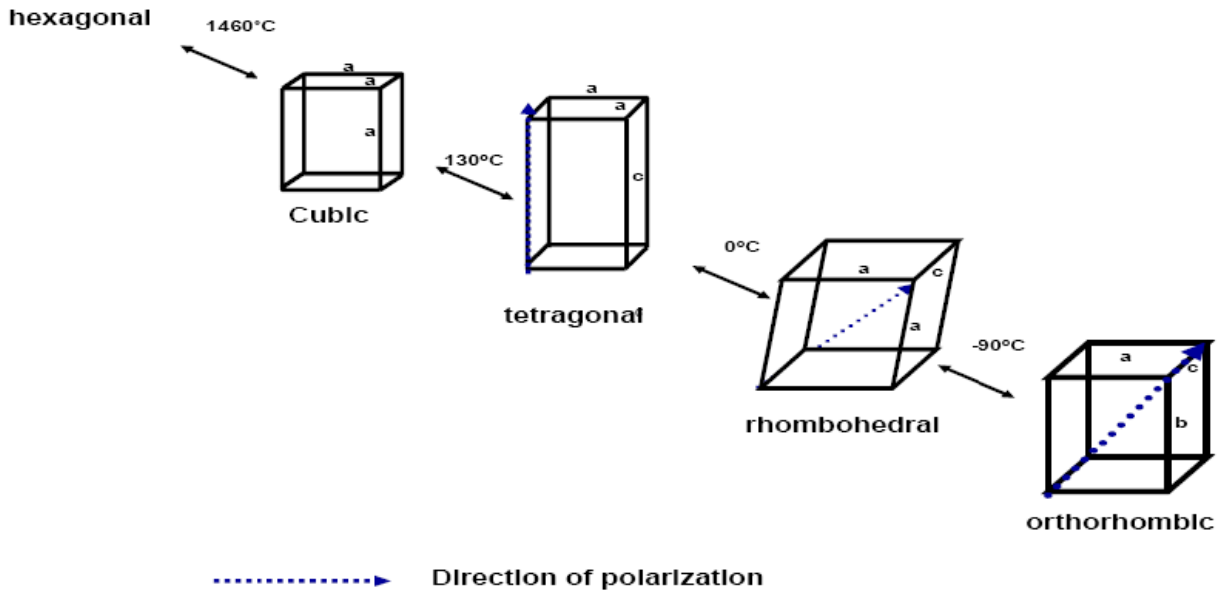

Fig 1.8 Phase diagram of $BaTiO_3$

Fig 1.8 shows hexagonal $BaTiO_3$ structure is stable above 1460^0C. Reconstructive hexagonal phase to cubic phase transformation occurs on cooling $BaTiO_3$ below1460^oC. Of utmost important parameter relating to its dielectric application is the ferroelectric - paraelectric transition which occurs at the Curie temperature (around 130^0C). At this temperature, paraelectric cubic $BaTiO_3$ transforms into the ferroelectric tetragonal structure following an elongation along an edge. The tetragonal phase is stable until 0^oC, where it transforms into the orthorhombic phase by elongation along a phase diagonal. Finally, there is a low temperature transition at - 90^oC where the orthorhombic phase transformed to the rhombohedral phase

It is used for this application due to its high dielectric constant and low dielectric loss. The values of the dielectric constant depend on the synthesis route, which means purity, density, grain size

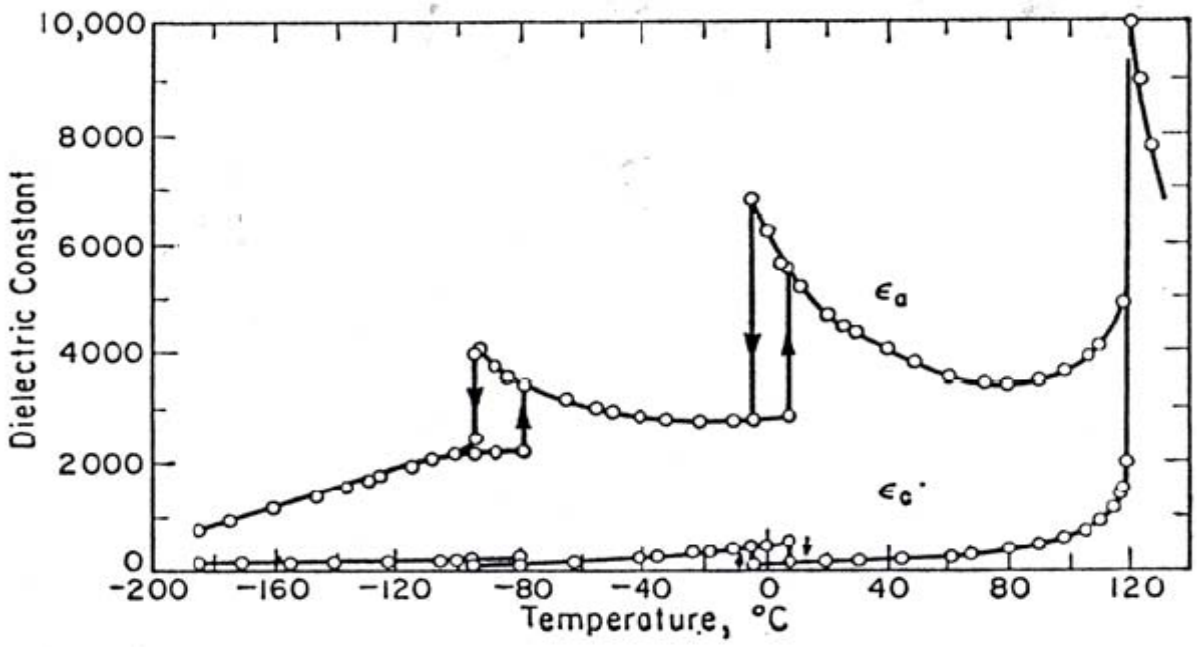

Fig. 1.9 Dielectric constants of $BaTiO_3$ as a function of temperature

etc [12]. The dielectric constant is also dependent on temperature, frequency and dopants.
Fig. 1.9 shows the temperature dependence of the dielectric constant measured with a small field along the pseudo-cubic edge. In this figure, only the values of the dielectric constant in the tetragonal phase have a clear meaning, as they were measured on carefully selected single-domain crystals with the proper orientation.

Incidentally, $BaTiO_3$ is not used in its true chemical form, but, rather, is combined with special additives to modify and improve its basic properties. The additives for $BaTiO_3$ transducers can be Sr^{2+} for varying the T_c downward from 130°C, Pb^{2+} for varying the T_c upward, Ca^{2+} for increasing the temperature range of stability of the tetragonal phase, and Co^{2+} for decreasing the high-electric-field losses without affecting the piezoelectric constants. Depressors, such as $Bi_2(SnO_2)_3$, $MgZrO_3$, $CaTiO_3$, $NiSnO_3$, as well as the shifters are added in small (1–8 wt%) quantities to the base $BaTiO_3$ composition to lower or depress the sharpness of the dielectric constant peak at the T_c, thus giving a flat dielectric constant–temperature profile [13].

1.5.2 Lead zirconate titanate (PZT) and lanthanum modified lead zirconate titanate (PLZT)

PZT is a solid solution of $PbZrO_3$ and $PbTiO_3$ and the compositions around $Pb(Zr_{0.52}Ti_{0.48})O_3$ are of technical importance. PZT and modified PZT are materials of choice for transducer applications [9, 14, 15] because they (1) possess higher electromechanical coupling coefficients than $BaTiO_3$, (2) have higher T_C values, which permit higher temperature of operation or higher temperature of processing during fabrication of the devices, (3) can be easily poled, (4) possess a wide range of dielectric constants, (5) are relatively easy to sinter at lower temperatures than $BaTiO_3$, and (6) form solid-solution compositions with many different constituents, thus allowing a wide range of achievable properties.

1.5.3 Strontium barium niobate ($Sr_xBa_{1-x}Nb_2O_6$)

Tungsten bronze structure ferroelectric material is $Sr_xBa_{1-x}Nb_2O_6$ (SBN, where $0.25 \leq x \leq 0.75$). Its potential applications is based on very attractive electro-optic [16], pyroelectric [17], photorefractive [18] and piezoelectric [19] properties. By changing the ratio between strontium and barium one may tune the system from a conventional ferroelectric (x<0.5) to an extreme relaxor (x>0.6) behaviour while maintaining the structure unchanged. In polycrystalline form most of the report is on the relaxor behavior of this material [20]. Its T_{ε_m} and and permittivity varies from 15-95^{o}C and 900-3500 with composition, [19,20] respectively. Abnormal grain growth during high temperature sintering restricts its applications in ceramic form [21].

It should be mentioned here that the abbreviation SBN used for $Sr_xBa_{1-x}Nb_2O_6$ should not be confused with the same abbreviation SBN often used for $SrBi_2Nb_2O_9$ (see Bismuth layer-structure ferroelectrics).

1.5.4 Bismuth layer-structure ferroelectrics

$Bi_4Ti_3O_{12}$-based system

The family of bismuth layer-structured ferroelectrics (BLSF) [22] is very attractive from the viewpoint of their applications because BLSF are characterized by their low ε, high T_c, and a large anisotropy in the electromechanical coupling factor (k_t/k_p or k_{33}/k_{31}) [11]. Therefore, the BLSF ceramics are seen as superior candidates for lead-free piezoelectrics for high-T_c piezoelectric sensors, filters, resonators and/or pyroelectric sensors with large figures of merit.

Bismuth titanate, $Bi_4Ti_3O_{12}$ (BIT), is a well-known BLSF material [23]. The BIT layer structure is characterized by bismuth oxide ($(Bi_2O_2)^{2+}$) layers positioned between perovskite-like layers. This crystal structure promotes a platelike morphology with the $(Bi_2O_2)^{2+}$ layers parallel to the plane of the platelets. BIT is monoclinic in the ferroelectric phase but is generally represented using an orthorhombic setting with the c-direction perpendicular to the layers and the major component of the spontaneous polarization in the a-direction of the perovskite plane. Cummins and Cross [24] reported anisotropic spontaneous polarizations in BIT single crystals (50 μC/cm^2 along the *a*-axis and 4 μC/cm^2 along the *c*-axis) [24]. On the other hand, fully reliable piezoelectric properties of BIT ceramics have not been reported because of some problems such as low resistivity and large coercive field [24].

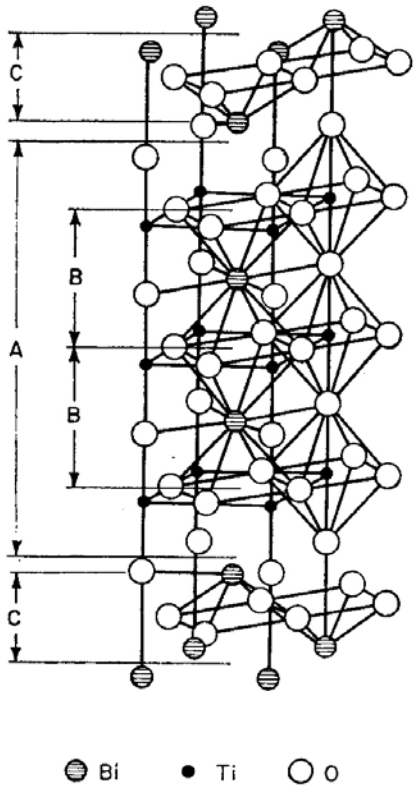

Fig.1.10 Crystal structure of $Bi_4Ti_3O_{12}$, C denotes $Bi_2O_2^{2+}$ layers and B denotes units of hypothetical perovskite structure. and A denotes the perovskite multiple layer height.

To solve these problems, Nb^{5+} and V^{5+} ions were doped into BIT ceramics to obtain higher resistivities [25,26]. The highest d_{33} of 20 pC/N was achieved with a composition corresponding to $Bi_4Ti_{2.86}Nb_{0.14}O_{12}$ with a T_c of 655^{o}C.

A few bismuth oxide layered perovskite materials, such as $SrBi_2Nb_2O_6$ (SBN), $SrBi_2Ta_2O_9$ (SBT), and $SrBi_2(Nb,Ta)_2O_9$ (SBTN), $SrBi_4Ti_4O_{15}$ have attracted an increasing attention in the research community, because they are fatigue-free and lead-free and possess ferroelectric properties independent of film thickness for FeRAM application. Layered perovskite ferroelectrics, however, suffer from two drawbacks: a relatively low remanent polarization and a high processing temperature. Recently, efforts have been made to enhance the properties of layered perovskite ferroelectrics by the addition or substitution of alternative ions [27,28].

1.6 Application of Ferroelectric materials

The applications for ferroelectric ceramics are manifold and pervasive, covering all areas of our workplaces, homes, and automobiles. Similar to most materials, the successful applications of piezoelectric, pyroelectric, ferroelectric, electrostrictive, and electrooptic ceramics and films are highly dependent on the relative ease with which they can be adapted to useful and reliable devices.

One category of applications for ferroelectric materials is that of high-dielectric-constant capacitors, particularly *Multilayer capacitor* (MLCs). MLCs are extremely important to our everyday lives in that they are essential to all of our currently produced electronic components, and, as such, they constitute a significant portion of the multibillion dollar electronic ceramics business as a whole. Typical applications include general-use discrete capacitors and MLCs, voltage-variable capacitors, and energy-storage capacitors. [13, 29,30]. Another application of ferroelectric material is $BaTiO_3$ based PTC ceramic possessing electrically conducting properties at room temperature and rather abruptly changing to a highly resistive material at some elevated temperature at T_c. Applications include switches, sensors, motor starter and controller [13].

Ferroelectric materials found applications in *electrooptics and photonics* due to their change in optical properties and ferroelectric polarization with an applied electric field. PLZT shutter and linear gate arrays found applications in flash goggles, cockpit viewing port, offset image setter, film writer and premier image enhancement systems [1, 13]. $LiNbO_3$ crystal is transparent from the band gap edge absorption at about 320 nm (~3.9 eV) up to the first infrared vibrational absorptions at a wavelength of about 5 μm (0.25 eV), covering all the visible and near infrared spectral regions. This provides a wide spectral window for photonic applications [31].

By far, the largest number of applications in ferroelectric ceramics remain associated with bulk materials, but a trend toward thin and thick films for some of these applications has recently been observed and has been steadily increasing in intensity. The importance of ferroelectrics for cooling has recently got an impetus. Ferroelectrics can be cooled by applying an electric field to them under certain conditions ("*electrocaloric effect*"). Recently, Mischenko et al. measured $\Delta T = 12$ K at 25 V across 350 nm of PZT film [32,33], which is sufficient to design a prototype cooler for computer mainframes.

The fact that ferroelectrics emit copious electrons (*electron emitter*) from their surfaces during switching has been known for many years. First discovered in Michigan by Rosenblum, this phenomenon was later investigated extensively at Centre Européen pour la Recherche Nucleaire (CERN) [34] and in France, Poland, Israel, and the United States. Currents of tens of amperes have been obtained with synchronized, monoenergetic pulse lengths of 100 ns to 1 μs. These are superior to thermionic cathodes in that the ferroelectrics have higher current densities and lifetimes and also have instant turn-on (thermionic cathodes require a warm-up) capability. This is an unexploited area for which commercial development of miniature high-power microwave devices could be made within a few years [35].

A *ferroelectric DRAM* (*FeDRAM*) film, because of its much higher dielectric constant, occupies much less wafer area than the normal SiO_2 capacitor, thus allowing much greater capacity memories to be fabricated on a given silicon wafer [36]. Ferroelectric memories are also nonvolatile. As memories become more dense in the future, the transition to ferroelectric films will become a necessity, and operating voltages for these memories will continue to decrease toward 1 V. At present, $(Ba,Sr)TiO_3$ (BST) film capacitors are the top contenders for these applications. The development of ferroelectric random access memory (*FeRAM*) films for nonvolatile memory applications, such as computer random-access memories, smart cards, and radio-frequency identification tags, is presently underway and has reached modest production levels for specific niche applications [36]. FeRAM films of several compositions, including PZT, PLZT, and $SrBi_2Ta_2O_7$ (SBT), are actively being investigated. Among these, SBT is, perhaps the material of choice in regard to switching fatigue. SBT materials, exhibiting little (<10%) fatigue up to 10^{12} switching cycles, have been developed; however, this value must be increased to ~10^{14} cycles before these films can be used in large-scale applications.

Thin-film ferroelectrics exhibit a large decrease in dielectric constant with application of modest voltages. This suggested that they could be used as the active *phase-shift element*s in phased-array radar. Unfortunately, the dielectric loss tangent in these films remains too large for acceptable insertion losses in such devices.

REFERENCES

1. A.J. Moulson and J.M.Herbert, Electroceramics-Materials-properties-applications Chapman and Hall, London, p.18, 52,277 (1990).
2. L. A. Shuvalov, J.Phys. Soc.Jpn., **28** [supplement], 38 (1970
3. A. K. Tagantsev, I. Stolichnov, N. Setter, J. S. Cross, and M. Tsukuda, Phys. Rev. B, **66**, 214109 (2002).
4. S-W Cheong and M Mostovoy, Nature Mater, **6,** 13 (2007).
5. R.E.Cohen, Nature, **358**, 136 (1992).
6. R. Seshadri and N. A. Hill, Chem. Mater., **13,** 2892 (2001).
7. A. P. Levanyuk and D. G. Sannikov, Sov. Phys. Usp., **17**, 199 (1974).
8. B. B. Van Aken, M. T. T. Palstra, A. Filippetti and N. A. Spaldin, Nature Mater., **3,** 164 (2004).
9. B. Jaffe, W. R. Cook Jr. and H. Jaffe, Piezoelectric Ceramics, Academic Press, NewYork, pp 7, 39, 46, 78,146,213-226 (1971).
10. W.J. Merz, Phys.Rev, **76,** 1221 (1949).
11. S.Elliot, The Physics and Chemistry of Solids, John Wiley and Sons, Chichester, p. 560 (1998)
12. W.Cao, and L.E.Cross, Phys.Rev.B, **44**, 5 (1991).
13. G. H. Heartling, J. Am. Ceram. Soc., **82,** 797 (1999).
14. G. Shirane, K. Suzuki, and A. Takeda, J. Phys. Soc. Jpn., **7**, 12 (1952)
15. B. Jaffe, R. S. Roth, and S. Marzullo, J. Appl. Phys., **25**, 809 (1954).
16. P. V. Lenzo, E. G. Spencer, and A. A. Ballman, Appl. Phys. Lett. , **11**, 23 (1967).

17. A. M.Glass, J. Appl. Phys., **40**, 4699 (1969).

18. M. D. Ewbank, R. R. Neugaonkar, W. K.Cory, and J. Feinberg, J. Appl. Phys., **62**, 374 (1987).

19. T. Volka, D. Isakova, V. Salobutina, L. Ivlevab, P. Lykovb, V. Ramzaevc and M.Wo¨hleckec, Solid State Commun.,**130,** 223 (2004)

20. M-S. Kim, J-H Lee, J-J Kim,H.Y. Lee and S-H Cho, J. Eur. Ceram.Soc., **22**, 2107 (2002)

21. N.S.VanDamme, A.E.Sutherland, L.Jones, K.Bridger and S.R.Winzer J.Am.Ceram.Soc.**74**, 1785 (1991)

22. T.Takenaka and H. Nagata J.Eur.Ceram Soc., **25**, 2693 (2005)

23. L. E. Cross and R. C. Pohanka, Mater. Res. Bull., **6**, 939 (1971).

24. S. E. Cummins and L. E. Cross, J. Appl. Phys., **39**, 2268 (1968).

25. H S Shulman, M. Testorf, D.Damjanovic and N.Setter, J.Am.Ceram.Soc., **79,** 3124 (1996).

26. Y. Noguchi, and M. Miyayama, Appl. Phys. Lett., **78**, 1903 (2001),.

27. C.A.de Araujo, J.D.Cuchlaro, L.D.McMillan, M.C.Scott and J.F.Scott, Nature, **374**, 627 (1995)

28. Y.Wu and G.Cao, J.Mater.Res., **15**, 1583 (2000)

29. G. Goodman, 'Ceramic Capacitor Materials', in Ceramic Materials for Electronics. Ed. by R. C. Buchanan. Marcel Dekker, New York, pp. 79–138 (1986).

30. M. Kahn, D. Burks, I. Burn, and W. Schulze, 'Ceramic Capacitor Technology'; Electronic Ceramics. Ed. by L. M. Levinson. Marcel Dekker, New York, pp. 191–274 (1988).

31. L. Arizmendi, phys. stat. sol. (a) **201**, 253 (2004).

32. J. F. Scott, Science **315**, 954 (2007).

33. A. S. Mischenko, Q. Zhang, J. F. Scott, R. W. Whatmore, N. D. Mathur, Science **311**, 1270 (2006).

34. H. W. Gundel, Ferroelectrics, **184**, 89 (1996).

35. B. Naranjo, J. K. Gimzewski, S. Putterman, Nature, **434**, 1115 (2005).

36. L. M. Sheppard, Am. Ceram. Soc. Bull., **71**, 85 (1992).

Chapter2

LITERATURE REVIEW

2.0 **Barium titanate synthesis methods**

Barium titanate ($BaTiO_3$) was synthesized through different techniques by various researchers. The selected techniques for synthesizing barium titanate depend on cost as well as applications. The quality of the powders is not only influenced by the synthesis route but also by the starting materials used. As miniaturization of electronic devices continues to demand smaller particle size powders with controlled morphology, the desired characteristics of the starting powder become a critical issue [1]. The successful synthesis of barium titanate powder with their unique dielectric properties largely depends on the purity and crystal structure that greatly influences final properties [2, 3].

2.1 Conventional solid-state reaction

Barium titanate can be prepared by a solid-state reaction that involves ball milling of $BaCO_3$ or BaO and TiO_2 which requires calcination of the mixture at high temperature. Some researchers reported that the needed calcination temperature was as high as 800 ^{o}C to 1200 ^{o}C [4-6], and also at 1300 ^{o}C [7]. Barium titanate powders prepared by a solid-state reaction are highly agglomerated, with a large particle size (2-5 μm) and high impurity contents due to their inherent problems such as high reaction temperature, heterogeneous solid phase reaction, which result in poor electrical properties of the sintered ceramics [8].

Manzoor et al [9] reported that the Size control of $BaTiO_3$ was prepared in the reaction between $BaCO_3$ and TiO_2. Smaller TiO_2 particles have higher surface area, resulting in faster initial reaction. The mechanically milled $BaCO_3$ particles accelerated the diffusion process and decreased the calcinations temperature. They reported that nano-sized $BaTiO_3$ particles with about 60 nm can synthesized by using the conventional solid-state reaction between $BaCO_3$ and TiO_2.

2.2 Chemical methods for barium titanate synthesis

Chemical synthesis of $BaTiO_3$ has grown up through different techniques such as sol – gel, coprecipitation, hydrothermal and polymeric precursor method. The advantage of chemical methods is the quasi–atomic dispersion of constituent components in a liquid precursor, which

facilitates synthesis of the crystallized powder with submicron particles and high purity at low temperatures. The properties of the powder depend on different preparation methods.

2.2.1 Sol-Gel method

Sol-gel is a method for preparing metal oxide glasses and ceramics by hydrolyzing a chemical precursor to form a sol and then a gel, which on drying (evaporation) and pyrolysis gives an amorphous oxide.

Wang et al [10] used two typical wet-chemistry synthesis methods such as stearic acid gel and acetic acid gel. Both the methods were prepared $BaTiO_3$ powder calcined at 550^0C by SAG and 800^0C by AAG respectively which has a cubic perovskite structure. They observed different grain size distributions within 25–50 nm for SAG and 50–80 nm for AAG. The particles were almost irregular in shape and agglomerate seriously due to high synthesis temperature in case of AAG. SAG has no Ba and Ti losses, and no halide anions and alkali-metal cations introduced or generated in the course of reaction, thus, SAG is one of most effective and convenient way to synthesize $BaTiO_3$ nanopowders.

Xueguang et.al [11] used sol-precipitation process which does not require further thermal treatment of the product, such as calcination or annealing due to enhance the homogeneity of crystals and crystal growth. However, single-crystal $BaTiO_3$ nanoparticles can be directly obtained at the low temperature of 80 ^{o}C and a strong alkaline condition rather than amorphous gel that often formed in the standard sol-gel process. They found nanoparticles with an average diameter of about 20 nm using Transmission electron microscopy.

Cheung et al. [12] prepared $BaTiO_3$ powders and films by a sol-gel method. This method involved the mixing of titanium isopropoxide and barium acetate in deionized water under continuous stirring at room temperature. They found crystallite size is around 20-35nm and the room temperature relative permittivity of the films (measured at 1 kHz) annealed at 700, 750, 800 and 850°C were 207, 225, 367 and 401 respectively. They also observed that the values of the remanent polarization, spontaneous polarization and coercive field of the film annealed at 850°C were 5mC/cm2, 10mC/cm2 and 70kV/cm, respectively.

Hwang et.al [13] synthesized spherical $BaTiO_3$ particles by the sol- gel method at 45°C. The (Ba–Ti) gel used as a starting material was prepared by aging mixtures of titanyl acylate with a

barium acetate aqueous solution. Potassium hydroxide (KOH) was used as a catalyst for the formation of $BaTiO_3$. They found fully crystallized spherical $BaTiO_3$ powder with a particle size of 40–250 nm, formed at the very low reaction temperature of 45°C.They also observed that the final particles formed via aggregation of the fine particles that seem to be the primary particles of bulk (Ba–Ti) gel.

2.2.2 Hydrothermal Method

The hydrothermal method is also used for synthesizing $BaTiO_3$ powder. Ciftci et al [14] synthesized $BaTiO_3$ powder by the hydrothermal method at temperatures between ~100-200 ^oC by reacting fine TiO_2 particles with a strongly alkaline solution (pH>12) of Ba $(OH)_2$. $TiCl_4$, titanium alkoxide and TiO_2 gels were used as titanium sources at reaction temperatures in the range of 100-400 ^oC. They found particle size of $BaTiO_3$ in the range of 50-400 nm.

Boulos et al [4] synthesized $BaTiO_3$ powders by the hydrothermal method using two different titanium sources $TiCl_3$ and TiO_2. The barium source was $BaCl_2 \cdot 2H_2O$. They synthesized $BaTiO_3$ at two temperatures, namely 150 ^oC and 250 ^oC. They observed that SEM micrographs of barium titanate powders show spherical highly crystallized elementary grains with sizes in the range 40-70 nm for samples prepared from $TiCl_3$ at 150 ^oC and 80-120 nm at 250 ^oC. The average particle size for powders obtained from TiO_2 at 150 ^oC or 250 ^oC was 40-70 nm.

Liu at al. [16] prepared $BaTiO_3$ by the microwave method and evaluated its sinterability, microstructure and dielectric properties in comparison to samples prepared by conventional hydrothermal processing. Starting reagents were Ba $(NO_3)_2$, $TiCl_4$ and KOH. All chemical reactions were conducted in a microwave digestion system. The system is controlled by pressure and the parameters which were varied include pressure (and thus, temperature) and time. They found that SEM analysis of powders prepared by both hydrothermal methods yielded a particle size of about 0.2 μm. Thus cubic $BaTiO_3$ powders can be prepared by the microwave method for 0.25 h, but in the case of conventional hydrothermal route for 2.5 h.

Guo et al. [17] observered that the microwave hydrothermal method can obtain the desired $BaTiO_3$ powder in a shorter time and at a lower temperature (30 min, 80 ^oC) than the conventional hydrothermal method (5h, 150 ^oC).

Sasirekha et al. [18] synthesized nanosized barium titanate powders by a hydrothermal method. They studied the effect of titania precursors on the phase transition of $BaTiO_3$ with respect to Ba/Ti ratio, reaction temperature, reaction time, and calcination temperature. They observed $BaTiO_3$ in pure cubic phase with spherical morphology with a lower calcination temperature, Ba/Ti ratio, reaction temperature, and time.

2.2.3. Mechanochemical synthesis

Stojanovic et al [19] prepared $BaTiO_3$ by mechanochemical synthesis, starting from barium oxide (BaO) obtained from thermally treated $BaCO_3$, according to the following reaction

$BaCO_3 \rightarrow BaO + CO_2$ in air at 900 ^{o}C/4h, and titanium oxide (TiO_2) in a rutile crystal form. Mechanochemical activation, i.e. mechanochemical synthesis was performed in a planetary ball mill in an air atmosphere for up to 4h, using a zirconium oxide vial and zirconium oxide balls as the milling medium. They identified strong agglomeration of powders after milling for 4h. $BaTiO_3$ powder consisted of particle agglomerates of varying size and morphology, with grains of a mostly rounded shape in the range of 20-50 nm.

Xue et al. [20] synthesized a perovskite $BaTiO_3$ phase in an oxide matrix that consists of BaO and TiO_2 by mechanical activation, without any additional heat treatment in a nitrogen atmosphere. They found that $BaTiO_3$ powder exhibits a well established nanocrystalline structure with crystallite size of ~ 14 nm and an average particle size of 20–30 nm for the activation-derived $BaTiO_3$ powder.

Miclea et al [21] synthesized single phase $BaTiO_3$ from BaO and TiO_2 by mechanochemical process, after 50 h of milling in a high energy ball mill. They found perovskite phase of $BaTiO_3$ powder with particle size 50 nm. They observed best dielectric properties in fine grained ceramics with average grain size of 2 μm, where the dielectric constant at room temperature was 5800 compared with only 1000 for coarse grained ceramics, with average grain size of 12 μm.

2.2.4 Combustion synthesis

Luo et al [22] prepared nanosized tetragonal barium titanate by low-temperature combustion synthesis process (LCS). They produced tetragonal $BaTiO_3$ with high purity at low ignition temperature (~300°C) and the crystalline size of the powder obtained was found to be less than 50 nm.

Won et al [23] synthesized tetragonal and submicron barium titanate particles from the BaO_2–TiO_2–C mixture through a low temperature isothermal heat treatment utilizing combustion synthesis technique. They found that precursor powder prepared by the combustion method easily transformed to the tetragonal $BaTiO_3$ starting from 700 °C. They also found that the formation of tetragonal $BaTiO_3$ powder at low temperature is conditioned by high chemical activity and specific characteristics of combustion products. $BaTiO_3$ specimens were found to possess high dielectric constant and low dissipation factor at room temperature.

Anuradha et al [24] studied the combustion synthesis of nanostructured barium titanate. Various samples of $BaTiO_3$ were prepared by the solution combustion of three different barium precursors (BaO_2, $Ba(NO_3)_2$ and $Ba(CH_3COO)_2$) and fuels such as carbohydrazide (CH), glycine (GLY) or citric acid (CA) in the presence of titanyl nitrate. They observed particle size of $BaTiO_3$ in the range of 10–50 nm , crystal structure in Cubic $BaTiO_3$ and crystallite size in the range of 50-60nm.

2.3 Molten salt Method

Mechanism of Molten salt synthesis

The reaction mechanism of a given phase in the MSS is little different from that of the solid-state reaction, as long as the salt intervenes in the formation reaction of the required phase are shown in fig 2.1 [15]

.

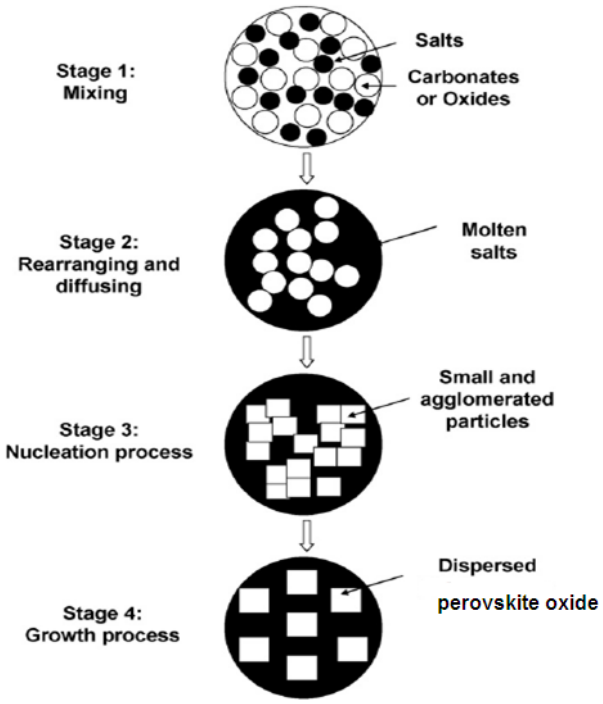

Fig. 2.1. Schematic illustration of the main processing stages in the MS method [15]

Oxides corresponding to a perovskite compound are mixed with one or two kinds of salt and then fired at a temperature above the melting point of the salt to form a flux of the salt composition. At this temperature, the oxides are rearranged and then diffused rapidly in a liquid state of the salt. With further heating, particles of the perovskite phase are formed through the nucleation and growth processes.

Gorokhovsky et al [25] studied the prepared $BaTiO_3$ by treatment of TiO_2 powder in molten mixtures of KNO_3–Ba $(NO_3)_2$–KOH. The products were characterized by different ratios of $BaTiO_3/TiO_2$. The rate of $BaTiO_3$ formation was not influenced by the temperature of treatment in the range of 450–550^{0}C. Lower temperatures and longer times of treatment are preferable because of the higher stability of nitrate ions in the melt. If the chemical composition of the product must be controlled, the large particles of barium polytitanates could be eliminated from the suspension by using fine filter paper.

Gopalan et.al [26] observed that the formation of solid solutions of $BaTiO_3$ –$SrTiO_3$ and $BaZrO_3$ –$SrZrO_3$ using a molten salt eutectic of NaOH–KOH as a solvent. Alkaline earth carbonates and titanium oxide were used as precursors for the titanate system, and alkaline earth carbonates and zirconium oxide were used as precursors for the zirconate system. The

calcination temperature was found to 573K for 12h. The molten salt serves as a solvent medium in which reaction kinetics are considerably faster compared to that in the solid state.

Rorvik et al [27] preapared $BaTiO_3$, $PbTiO_3$, and $Na2Ti_6O_{13}$ nanorods by molten salt synthesis route to elucidate the role of volatile chlorides. A precursor mixture containing barium (or lead) and titanium was annealed in the presence of NaCl at 760 or 820 °C. The main products were respectively isometric nanocrystalline $BaTiO_3$ and $PbTiO_3$. They found that NaCl reacted with BaO (PbO) resulting in loss of volatile $BaCl_2$ ($PbCl_2$) and formation and preferential growth of titanium oxide-rich nanorods instead of the target phase $BaTiO_3$ (or $PbTiO_3$).

Jeffrey et al [28] synthesized $BaTiO_3$ and $SrTiO_3$ nanorods by solution-phase decomposition of bimetallic alkoxide precursors in the presence of coordinating ligands. They observed that the reaction yields well-isolated nanorods with diameters ranging from 5 to 60 nm and lengths reaching up to >10 μm. These nanorods are composed of single-crystalline cubic perovskite $BaTiO_3$.

Mao et al [29] synthesized pure perovskite phase $Ba_{0.70}Sr_{0.30}TiO_3$ (BST) powders by molten-salt method in NaCl–KCl flux at a low temperature of 850^0C for 2 h, which is 300 ^{o}C lower than that of the conventional solid-state reaction. This process involved mixing of the raw materials and salts in a certain proportion. Subsequent calcining of the mixtures led to BST powders at 800–900^0C.

Thirumal et .al [30] synthesized perovskite related dielectric oxides of the formula Ba ($Zn_{1/3}Nb_{2/3}$) O_3, Ba ($Mg_{1/3}Nb_{2/3}$) O_3 and Ba ($Zn_{1/3}Ta_{2/3}$) O_3 by the NaCl–KCl molten salt (flux) method at low temperatures of 900^0C for 3 or 6 h. Sintering at 1000^0C retained the cubic structure and generated minor amount (~10%) of $Ba_5Nb_4O_{15}$ at 1300^0C in addition to the main cubic phase for the niobium compounds. They observed that large grain sizes (upto 10μm) in some of the samples were obtained by the molten salt method.

Liu et.al [31] synthesized single crystalline $BaTiO_3$ nanoparticles starting from $BaCO_3$ and TiO_2 by a composite-hydroxide-mediated method. They found all $BaTiO_3$ samples of cubic phase with size from 70 to100 nm under different reaction temperature (165–220 °C) and time (24–72 h); higher temperature and longer time clearly favored the increase of particle size.

Yuanbing et. al [32] prepared single-crystalline $BaTiO_3$ nanowires and $SrTiO_3$ nanocubes with a novel and simple one-step solid-state chemical reaction in the presence of NaCl at 820^0C

and a nonionic surfactant(NP9). They scaled up this process to produce grams of single-crystalline $BaTiO_3$ and $SrTiO_3$ nanomaterials. They found nanowires of about 50-80 nm in diameter, and their lengths range from 1.5 μm to even longer than 10 μm. They also observed the purity and crystallinity of the as-prepared samples using powder XRD.

Zhou et. al [33] synthesized single-crystalline perovskite $BaZrO_3$ submicrometer-sized particles using a simple, scaleable molten salt method. Cubic $BaZrO_3$ particles edge length measuring 120 (25 nm based on a measurement of 50 particles) could be prepared by heating precursors in a NaOH-KOH mixture (49.2:50.8 mol %; mp 170 °C) to 720 °C. Annealing of this sample at this temperature ensued for 30 min, in the presence of NaOH/KOH (49.2: 50.8 mol % ratio; mp 170 °C) as the eutectic salt mixture, $BaZrO_3$ with a weight percentage of almost 100% could be generated at rather low temperatures (e.g., 720 °C). They studied molten salt synthesis (MSS) of $BaZrO_3$ submicrometer-sized particles and also the effects of different parameters, such as salt, surfactant, reaction temperature, reaction time, precursor type, amount of salt, heating/cooling rate, and molar precursor ratio, on the resultant product purity, size, shape, and morphology.

2.4. Sintering Behavior

Wang et al [34] investigated the preparation of bulk dense nanocrystalline $BaTiO_3$ ceramics using an unconventional two-step sintering strategy, which offers the advantage of not having grain growth while increasing density from about 73 to above 99.6%.The kinetics of unconventional two-step sintering method exploits the different kinetics between densification diffusion and grain boundary mobility. Using this method, bulk dense ceramics with a grain size of 8–10 nm was obtained successfully at a very low sintering temperature.

Ying et al [35] prepared nanometer-scale barium titanate ($BaTiO_3$) powders via a process consisting of chemical dispersion and physical grinding/mixing. The nano-$BaTiO_3$ was sintered at the temperatures ranging from 1100 to 1300^0C for various time spans. The $BaTiO_3$ sample sintered at 1100 ◦C for 6 h possesses relatively small grain sizes (about 140 nm), high density (about 95% T.D.) and distinct room-temperature dielectric properties (dielectric constant = 8000; dielectric loss = 5×10−3).

Lin et al [36] observed direct grain growth and densification of $BaTiO_3$ ceramics in a TEM equipped with an *in-situ* installed heating platform. Polotai et al [37] developed a novel approach to pressureless sintering based on the combination of rapid-rate sintering, rate controlled sintering, and two-step sintering under a controlled atmosphere. This combined sintering method facilitates control of grain and pore morphology. The application of this sintering approach for pure nanocrystalline barium titanate powder enables the suppression of grain growth during the intermediate and final stages of sintering and the production of fully dense ceramics with 108 nm grain size. The grain growth factor was 3.5, which was three and 17 times smaller than rate-controlled and conventional sintering, respectively.

2.5. Dielectric Behavior

Shi et al [37] studied the dielectric properties of barium titanium ceramics fabricated with nano-size fine powders (about 40 nm) with that fabricated with micro-size coarse powders (about 2 mm). They fabricated three kinds of ceramics; one using pure nano-size fine powders, the other using pure micro-size coarse powders, and the third using the combination of both. The sintering temperature of the ceramics with pure nano-size fine powders is 150^0C lower than that with pure micro-size coarse powders. For the same sintering conditions, the relative density of the ceramics increases with the amount of nano-size fine powders. The grain size of the ceramics body with pure micro-size coarse powder is about 5 mm, but that of pure nano-size fine powder is about 1 mm. The room temperature dielectric constant of the ceramics increases with the increasing of the amount of nanosized fine powder. For pure nano-size fine powders, the room temperature dielectric constant is about 5000, and that of micro-size coarse powders is about 2200.

Sun et al [38] investigated the size effect in barium titanate ($BaTiO_3$) both experimentally and theoretically. They directly prepared tetragonal BaTiO3 powders with average sizes from 80 to 420 nm by different hydrothermal methods. They found that tetragonality of the hydrothermal BaTiO3 decreases with decreasing particle size, which exhibited a dependence on the synthesis method. They predicted a maximum permittivity of $BaTiO_3$ over 16000 around the room-temperature and critical size of ~70 nm. The prediction was in good accordance with the experimental data reported.

Gao et al. [39] studied the dielectric behavior of $BaTiO_3$ ceramices as a function of grain size. They found that the grain size of the $BaTiO_3$ ceramics has a strong influence on the

permittivity and dissipation loss. Room temperature permittivity of the sample (<0.5 μm) showed relatively low values (2800) compared with those for ceramics sintered at 1250 °C, consisting of larger grains (≈1 μm). The lower permittivity was attributed to an incomplete development of the tetragonal structure.

Park et al [40] used various particle sizes of starting barium titanate in order to examine effect of grain size and external stress on the dielectric temperature characteristics of barium titanate. The grain size was proportional to the particle size of starting barium titanate. The dielectric temperature characteristics of the small grains (< 4 μm) was less sensitive to the grain size in comparison with those of the large grains (> 4 μm), which was attributable to the internal stress. Moreover, it was suggested that stress is one of the origins of diffuse phase transition (DPT).

Arlt et. al[41] studied dielectric properties, lattice and microstructure of ceramic $BaTiO_3$ showing grain sizes of 0.3- 100 μm . At grain sizes <10 μm, the width of ferroelectric 90°domains decreases proportionally to the square root of the grain diameter. The decreasing width of the domains can be theoretically explained by the equilibrium of elastic field energy and domain wall energy. The smaller the grains, the more the dielectric and the elastic constants are determined by the contribution of 90° domain walls. The permittivity below the Curie point showed a pronounced maximum εr ~5000 at grain sizes 0.8-1 μm. At grain sizes <0.7 μm the permittivity strongly decreases and the lattice gradually changes from tetragonal to pseudocubic.

Wada et al [42] measured the dielectric constant of barium titanate ($BaTiO_3$) fine particles from 17 to 1,000 nm and found that certain particle size possesses a maximum dielectric constant. The sizes with maximum dielectric constants were strongly dependent on preparation methods. When BaTiO3 fine particles were prepared in vacuum of 10-20 torr, a dielectric maximum of 15,000 was observed at 70 nm. On the other hand, when $BaTiO_3$ fine particles were prepared in air, a dielectric maximum of 5,000 was observed at 140 nm. Structure refinement of $BaTiO_3$ particles using a Rietveld method indicates that all of $BaTiO_3$ particles were composed of two parts; (a) surface cubic layer and (b) bulk tetragonal layer. Moreover, a thickness of surface cubic layer for $BaTiO_3$ particles prepared in vacuum was much thinner than that for $BaTiO_3$ particles prepared in air.

Begg et al [43] studied the room-temperature tetragonal-to-cubic transformation in $BaTiO_3$ powders with decreasing particle size, using materials prepared mainly by hydrothermal methods. It is observed that hydrothermal BaTiO3 powders exhibit a uniform particle size distribution. The tetragonal-to-cubic transformation temperature was found to lie in the range of 121°±3 °C for BaTiO3 powders with room temperature values >1.008.

Li et al [44] showed that clustering is an important effect on the tetragonal-cubic transformation of barium titanate ($BaTiO_3$) particles. Small particles that would be cubic, are tetragonal if they are in a cluster. The effects of clustering had been studied on the c/a ratio of the particles and the enthalpy change (ΔH), of transition as a function of particle size. The c/a ratio and the value of ΔH both decrease at a smaller particle size than those which are observed in samples where clustering is minimal. The results were consistent with the observation that very small grains in polycrystalline samples can remain tetragonal even though the grain size is so small that it would be cubic if it were an individual particle. The transition temperature, T_C, on the other hand, is insensitive to the particle size, which is similar to the observation in polycrystalline $BaTiO_3$ that Tc is insensitive to the grain size. The observed clustering effect is suggested to result from the reduction of depolarization energy of particles in clusters.

2.6 Summary

The preparation of $BaTiO_3$ powders by using solid state reaction requires high calcination temperature (800-1100^{0}C) and sintering temperature above 1300^{0}C. Barium titanate powders prepared by this process are highly agglomerated, with a large particle size (2-5 μm) and considerable impurity content found due to their inherent problems such as high reaction temperature, heterogeneous solid phase reaction, which result in poor electrical properties of the sintered ceramics.

The $BaTiO_3$ powder has been synthesized by sol gel method with calcination temperature 550-800^{0}C and sintering temperature 1100-1300^{0}C. The particle size found in the range of 25-80nm and dielectric constant 500-800. In combustion synthesis, the particle size was found around 50 nm for the powders calcined at 700^{0}C. In the hydrothermal method, processing temperature lies in the range of 100-400^{0}C. The particle size was found to be in the range of 40-400nm and sintering temperature of 1250^{0}C for 10 to 20 h. The dielectric constant was found nearly 6800 at

1 kHz .Materials prepared by these methods are of homogeneous, phase pure with finer particle size but of low density; it is a difficult task in particular to get dense $BaTiO_3$ ceramic. All of these methods are based on solution processes, they yield relatively small quantities of the desired nanostructures, and furthermore, in most cases, extremely toxic and unstable organometallic precursors are employed.

The $BaTiO_3$ powder has been synthesized by mechanochemical route. The mixtures of raw materials were milled for 50 h in high energy ball mill. The average particle size obtained was of 20-50nm. The dielectric constant has been observed to be 2500 for 10 kHz. In mechanochemical process high energy milling consume more energy and there is also chance of contamination.

The $BaTiO_3$ were prepared by molten salt method using different kind of salts such as NaCl, eutectic mixture of KNO_3–$Ba(NO_3)_2$–KOH and the powder was calcined in the range of 450-820^{0}C. But there are no reports on other salt system synthesis, sintering and dielectric properties of this powder.

Different other materials were also synthesized by the molten salt method using the eutectic mixture of NaOH–KOH and KCl-NaCl. The particle Size found in these methods was of 70-100nm depending upon the salt system. But there are no reports on sintering and dielectric properties of other salt system.

REFEREENCES

1. Lee B.I., Wang M., Yoon D., Hu M., J. Ceram. Proc. Research, 4 (2003) 17.
2. Haertling G.H., J. Am. Ceram. Soc., 82 (1999) 797.
3. Vinothini V., Singh P., Ceram. Int. 32 (2006) 99.
4. Boulos M., Guillement-Fritsch S., Mathieu F., Durand B., Lebey T., Bley V. Solid State Ionics 176 (2005) 1301.
5. Potdar H.S., Deshpande S.B., Date S.K., Mater. Chem. Phys. 58 (1999) 121.
6. Simon-Seveyrat L., Hajjaji A., Emziane Y., Guiffard B., Guyomar D., Ceram. Int. 33 (2007).
7. Ristic M.M., Milosevic S.Dj, Mechanical Activation of Inorganic Materials, Monographs, Belgrade, (1998).
8. Wu Long, Ming-Cheng Chure, King-Kung Wu, Wen-Chung Chang, Ming-Ju Yang Wei-Kuo Liu , Menq-Jion Wu Ceramics International 35 (2009) 957–960.
9. Manzoor U. and.Kim D.K J. Mater. Sci. Technol., Vol.23 No.5, 2007.
10. Wang L., Liu L., Xue D., H. Kang, C. Liu, J. Alloys Comp. 440 (2007) 78.
11. Xueguang. He ,Fan Guangneng, , Huangpu Lixia ,Journal of Crystal Growth Volume 279, Issues 3-4, 1 June 2005, pp 489-493.
12. Cheung M.C., Chan H.L.W., Zhou and Q.F.. Choy C.L Nano Structured Materials, Vol. 11, No. 7, pp. 837–844, 1999.
13. Un-Yeon Hwang, Hyung-Sang Park, and Kee-Kahb Koo *J. Am. Ceram. Soc.,* 87 [12] 2168–2174 (2004).
14. Ciftci .E., Rahaman M. N. Journal Of Materials Science 36 (2001) 4875 – 4882.

15. Yoon Kihun, Cho Yong Soo, Kang Dong Heon "Journal of Materials Science 33 (1998) 2977-2984.
16. Liu Shi-Fang, Isaac Abothu Robin , Komarneni Sridhar "Materials Letters 38(1999).344–350.
17. Guo L., Luo H., Gao J , Jianfeng Yang, Materials Letters 60 (2006) 3011
18. Sasirekha Natarajan, Rajesh Baskaran *Ind. Eng. Chem. Res.*, 2008, 47 (6), 1868-1875.
19. Stojanovic B.D.,. Jovalekic C, Vukotic V., Simoes A.Z.,. Varela J.A, Ferroelectrics, 319 (2005) 65.
20. Xue Junmin, Wang John, and Wan Dongmei *J. Am. Ceram. Soc.,* 83 [1] 232–34 (2000).
21. Miclea C., Tanasoiu C., Spanulescu I., Miclea C.F.,. Gheorghiu A, Amarande L., Cioangher M., 48 (1997) 237–241.
22. Luo Shaohua, Tang Zilong, Yao Weihua and Zhang Zhongtai, " Microelectronic Engineering Volume 66, Issues 1-4, April 2003, Pages 147-152.
23. Won H.I.,. Nersisyan H.H and Won C.W.,Materials Letters Volume 61, (2007), Pages 1492-1496.
24. Anuradha T.V., Ranganathan S., Mimani Tanu and Patil K.C Scripta mater. 44 (2001) 2237–2241.
25. Gorokhovsky A.V., Escalante-Garcia J.I., Sa´nches-Monjara´s T., Vargas-Gutierrez G. Materials Letters 58 (2004) 2227–2230.
26. Gopalan Srikanth, Mehta Karun, and Virkar Anil V. Journal of materials research 11:88, 1863-1865.
27. Rørvik Per Martin, Lyngdal Tone, Sæterli Ragnhild, Antonius Helvoort T. J. van, Holmestad Randi, Grande Tor, and Einarsrud Mari-Ann, "Inorg.Chem (2008),47,3173-3183
28. Jeffrey J. Urban, Wan Soo Yun, Qian Gu, and Hongkun Park "Synthesis of Single-Crystalline Perovskite Nanorods Composed of Barium Titanate and Strontium Titanate" *J. Am. Chem. Soc.*, 2002, 124 (7), 1186-1187.
29. Mao Chaoliang, Wang Genshui, Dong Xianlin, Zhou Zhiyong, Zhang Yuanyuan" Materials Chemistry and Physics 106 (2007) 164–167.
30. Thirumal M., Jain P., Ganguli A.K. Materials Chemistry and Physics 70 (2001) 7–11

31. Miao Jing, Hu Chenguo, Liu Hong , Xiong Yufeng ., Materials Letters 62 (2008) 235–238.

32. Mao Yuanbing, Banerjee Sarbajit, and Wong Stanislaus S. American Chemical Society (2003) 125, 15718-15719.

33. Zhou Hongjun, Mao Yuanbing, and Wong Stanislaus S. *Chem. Mater.* 2007, *19,* 5238-5249.

34. Wang X-H., Deng X-Y., Zhou H., Li L-T and Chen I-W., Journal of Electroceramics doi:10.1007/s10832-007-9143-1

35. Ying Kuo-Liang, Hsieh T.-E. Materials Science and Engineering B 138 (2007) 241–245

36. Shi Jian-Lin, Deguchi Yoichi and Sakabe Yukio, Journal of Materials Science, Volume 40, Number 21 / November, 2005.

37. Polotai Anton, Breece Kristen, Dickey Elizabeth, and Randall Clive, J. Am. Ceram. Soc., 88 [11] 3008–3012 (2005)

38. Sun, W. Journal of Applied Physics 100 (8), 2006

39. Gao L.J., Liu X.L., Zhang J.Q., Wang S.Q. and Chen J.F., Mater. Chem. Phys. **88** (2004), p. 27.

40. Park Y. and Song S.A., Mater. Sci. Eng. B **47** (1997), p. 28

41. Arlt G., Hennings D., De With G. (1985) Journal of Applied Physics, 58 (4), pp. 1619-1625.

42. Wada S., Hoshina T., Yasuno H., Ohishi M., Kakemoto H., Tsurumi T., Yashima M.

Ceramic Transactions 174, pp. 15-26 (2006)

43. Begg, Bruce D., Vance Eric R., Nowotny Janusz (1994) Journal of the American Ceramic Society, *77* (12), pp. 3186-3192.

44. Li X., Shih W.-H. (1997) Journal of the American Ceramic Society, 80 (11), pp. 2844- 2852.

Chapter-3

OBJECTIVE

3.0 Objective

Oxide materials with perovskite structure having the general formula ABO_3 form the backbone of the ferroelectrics industry. Since long, $BaTiO_3$ has been known to show useful ferroelectric and piezoelectric properties. Ferroelectric $BaTiO_3$ fine particles have been used as raw materials of dielectric devices such as multilayered ceramic capacitors (MLCCs). Recently, with the miniaturization of electronic devices, the downsizing of MLCC has been developed and accelerated. As a result, it is expected that the thickness of dielectric layers in MLCC soon will become less than 500 nm. Consequently, the particle size of the required $BaTiO_3$ raw materials will decrease from a few hundred nanometers to a few tens of a nanometer.

$BaTiO_3$ with a high permittivity is essential to enhance the volumetric efficiency of multi-layer ceramic capacitors (MLCCs) and depressed Curie peak is necessary for temperature stability. For the development of future MLCCs as well as other nanodevices, $BaTiO_3$ nanoparticles should be handled and utilized. The critical size is where the crystal structure of $BaTiO_3$ shifts from the cubic to the tetragonal phase approximately 16 nm (based on empirical estimation). Experimentation has shown that the critical size ranges from 25 to 190 nm, depending on the preparation method. Production of $BaTiO_3$ powder with particle size in between the above mentioned range is a difficult task for material researcher.

Previous works in synthesizing this material have involved a number of different routes. While all of these methods are based on solution processes, they yield relatively small quantities of the desired nanostructures, and furthermore, in most cases, extremely toxic and unstable organometallic precursors are employed. Thus, the development of gram-scale and environmentally friendly synthetic methods with reproducible shape control is of paramount importance if the full potential of these materials is to be realized. Molten salt synthesis (MSS) method, in particular, is one of the simplest, most versatile, and highly cost-effective approaches available for obtaining crystalline, single phase nanoscale material at lower temperatures.

Earlier works emphasized on only synthesis of nanorod and nanocube of $BaTiO_3$ by molten salt method at a temperature of 800^oC using NaCl as salt system. But there are no reports on other salt system synthesis and sintering and dielectric properties of this powder.

In the present work synthesis of phase pure nanosize $BaTiO_3$ has been carried out by Molten Salt Synthesis (MSS) method. The following work has to be done to optimize the phase purity, morphology, particle size, sintered density and dielectric properties of $BaTiO_3$ powders:

1. Effect of different eutectic salt mixture namely NaCl-KCl, LiCl-KCl, and NaOH-KOH has to be studied on phase purity of $BaTiO_3$.
2. Optimization of different process parameters that are holding temperature, time on phase evolution, crystallite size and tetragonality in $BaTiO_3$.
3. Powder morphology of $BaTiO_3$
4. Effects of different salt system synthesized powder on the densification behavior of $BaTiO_3$.
5. Dielectric behavior of the sintered $BaTiO_3$.

Chapter 4

EXPERIMENTAL PROCEDURE

4.0 EXPERIMENTAL PROCEDURE

4.1 powder synthesis

Barium titanate powders were synthesized by molten salt synthesis route. The molten salts, used in these experiments were eutectics of NaOH -KOH (170^{o}C) with Na/K molar ratio 49.2/50.8, KCl–NaCl (658^{o}C) with Na/K molar ratio 50/50 and LiCl-KCl (355^{o}C) with Li/K molar ratio 59.2/39.8 that has been found from phase diagram (fig 4.1).

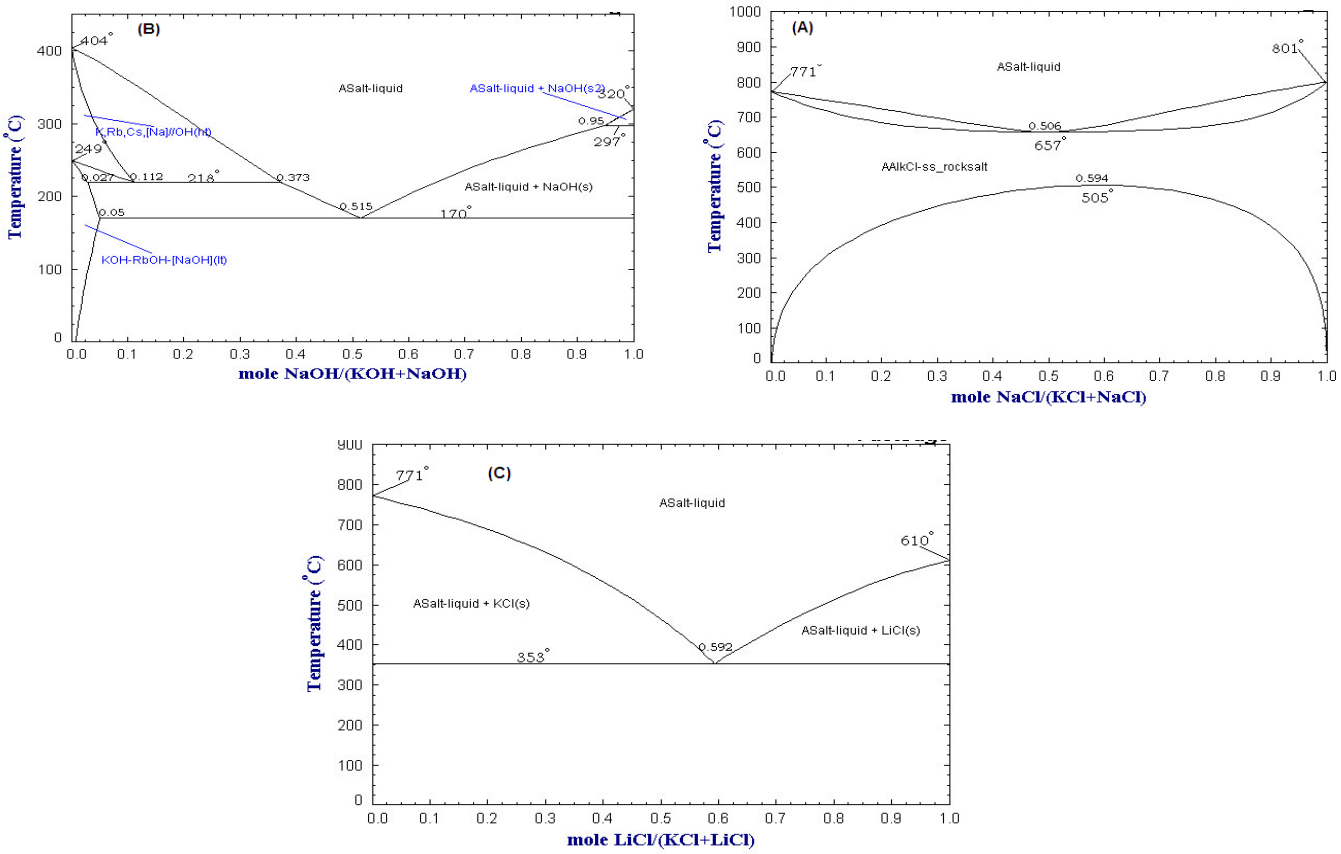

Fig 4.1 The systematic Phase diagram of various salt (a) NaOH-KOH (b) NaCl-KCl (c) KCl-LiCl system.

Reagent grade $BaCO_3$, TiO_2, NaCl, KCl, NaOH, KOH and LiCl were used as precursor materials. Stoichiometric amount of $BaCO_3$, TiO_2 powders were mixed with eutectic composition of NaCl-KCl in the molar ratio of (1:1:20). The powder mixtures were homogeneously mixed using reagent grade isopropyl alcohol in an agate mortar. The mixture was then put into an alumina crucible and heat treated at 700-800^{0}C for 2-6 hours. Then calcined powders were washed with hot deionized water until no Cl^- was detected by using $AgNO_3$ solution. The powders were dried in an oven at 100^{0}C.

Stoichiometric amount of $BaCO_3$, TiO_2 powders were mixed with eutectic composition of NaOH-KOH in the molar ratio (1:1:20). The powder mixtures were homogenized, the mixture were calcined at 175-500^{0}C for different hours. Then Calcined powers were washed with hot deionized water until no OH^- was detected by using pH meter (~7).Then powder were dried in an oven at 100^{0}C.

Stoichiometric amount of $BaCO_3$, TiO_2 powders were mixed with eutectic composition of LiCl-KCl in the molar ratio (1:1:20). The mixture was heat treated at 500^{0}C for two hours. Then Calcined powders were washed with hot deionized water. Then powders were dried in an oven at 100^{0}C. The flow chart for the powder synthesis is given in Fig. 4.2.

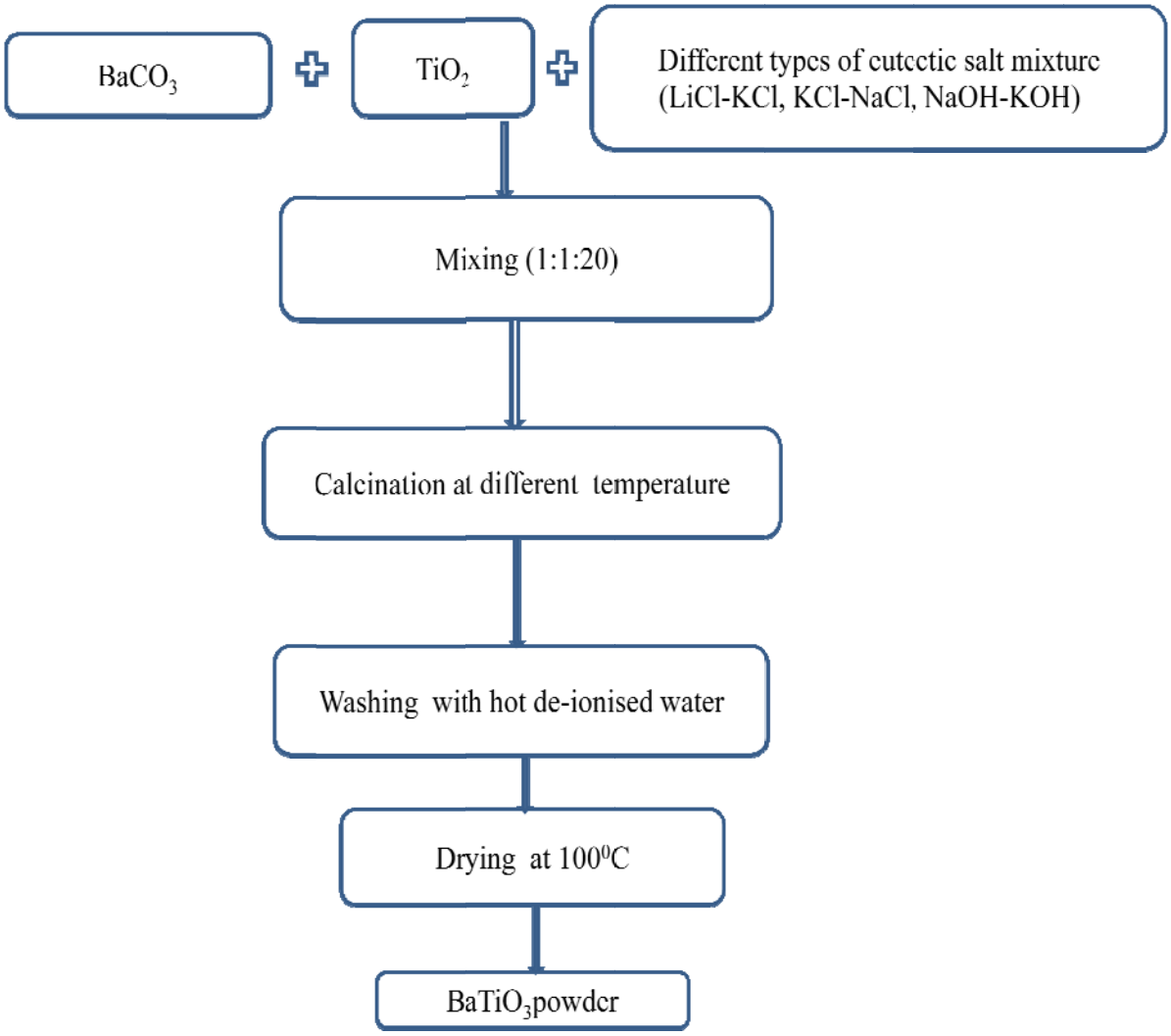

Fig 4.2 The process for the preparation of $BaTiO_3$ powders by molten salt route.

4.2. Powder Characterization

4.2.1 Phase analysis of calcined powder

The phase evolution of calcined powder as well as that of sintered samples was studied by X-ray diffraction technique (Philips PAN analytical, The Netherland) using Cu Kα radiation. The generator voltage and current was set at 35 KV and 25 mA respectively. The samples were scanned in the 2θ ranges 15 to 70^0C range in continuous scan mode. The scan rate was 0.04^o/sec. Phases present in the sample has been identified with the search match facility available with Philips X'pert high score software.

The crystallite size of the calcined powders was determined from X-ray line broadening using the Scherrer's equation as follows:

$$t = \frac{o.9\lambda}{B cos\theta} \qquad \text{---------- (1)}$$

Where,

t = crystallite size,

λ = wavelength of the radiation,

θ = Bragg's angle and

B = full width at half maximum

4.2.2 Particle Size Analysis

A laser diffraction method with a multiple scattering technique has been used to determine the particle size distribution of the powder. It was based on Mie-scattering theory. In order to find out the particles size distribution the $BaTiO_3$ powder was dispersed in water by horn type ultrasonic processor [Vibronics, model:VPLP1].Then experiment was carried out in computer controlled particle size analyzer [ZETA Sizers Nanoseries (Malvern Instruments Nano ZS)] to find out the particles size distribution.

4.2.3 Powder surface area measurement

The powders were oven dried at 100^{o}C overnight before analysis. BET surface area analysis was done by AUTOSORB 1, Quantachrome. The analysis was done by computer controlled programme.

Average Particle Size = (6 / BET surface area X Density) X 1000

Average Particle Size = (nanometers)

surface area = (m^2/g)

Density = (g/cc)

4.2.4 TEM Analysis

Specimens for transmission electron microscopy (TEM) and high resolution TEM (HRTEM) were obtained by drying droplets of $BaTiO_3$ samples from an acetonic dispersion onto 300 mesh

Cu grids, coated with a lacey carbon film. TEM images were taken at an accelerating voltage of 120 kV on a JEOL instrument.

4.2.5 Preparation of Bulk Sample

Various Calcined powder were mixed with 3 wt. % PVA (Poly Vinyl Alcohol) binder with the help of mortar and pestle. The binder mixed powder was compacted to give a desired shape for further characterization. The binder mixed powders were pressed uniaxially in a HC-HCr die into cylindrical pellets (12 mmΦ, 3mm high). The uniaxial pressing was done at 4 ton in a hydraulic press (4T,carver Inc ,USA). A holding time of 120seconds was given for pressing of each sample. The pressed green compacts were sintered in air with a heating rate of 3°C/min at the temperature ranges 1200 -1235^{0}C with a holding time of 3 hours in electrical furnance. The bulk density and apparent porosity of the sintered specimen were measured by Archimedes Principle.

4.2.6 Microstructure Analysis

Microstructure of sintered pellets has been studied using Scanning Electron Microscope (JEOL -JSM 6480LV). The generator voltage was 15 kV. Polished samples were prepared with Buehler, Ecomet 3; Automet 3 untill mirror finished is attained. The polished surface of the sample was then thermal etched at a temperature 100^{0}C below the sintering temperature for one hour.

4.2.7 Dielectric measurement

For dielectric measurement sample have been prepared by electroding with silver paste. The silver paste coated samples were cured at 500^{o}C for half an hour. Dielectric measurement has been carried out using Solatron S1 1260 Impedance /Gain-phase analyzer in standalone mode. The frequency range for the dielectric measurement was varied in the range of 100 Hz to 1MHz. Dielectric behavior has also been studied as a function of temperature.

Ferroelectric hysteresis loops were measured using an LC precision ferroelectric tester.

Chapter 5

RESULTS AND DISCUSSION

5.1 RESULTS AND DISCUSSIONS

The novelty of our specific approach can be summarized as follows. To the best of our knowledge, this is the first study to systematically probe parameter control in the molten salt synthesis of submicrometer-sized perovskite particles with the aim of reliable and reproducible size, shape, and composition control. Second, whereas Gopalan et al. [1] have formed solid solutions of $BaZrO_3$-$SrZrO_3$ using the molten salt eutectic of NaOH-KOH as a solvent, no one has reported the synthesis of either nanometer- or micrometer-sized $BaTiO_3$ particles using this particular eutectic solvent.

Molten salt method is a powerful tool to study $BaTiO_3$ at low temperature phase equilibrium. The molten salt serves as a solvent medium in which reaction kinetic are considerably faster compared to that solid state. The large numbers of molten salt system are available but we have to identify suitable salt system. In this case three salt systems are chosen to prepare the $BaTiO_3$.

Synthesis of $BaTiO_3$

$BaTiO_3$ Powder has been synthesized using three types of salt system as discuss. The phase evolution of powder and sinter sample, sintering behaviour, microstructure analysis, Dielectric behavior etc. discuss as follows.

5 .2. Phase analysis of calcined $BaTiO_3$ powder

(A) NaOH-KOH salt system

Fig 5.1 shows the XRD pattern of $BaTiO_3$ powder synthesized using NaOH –KOH salt system after calcination at a temperature ranging from 175 to 500^0C for 2h. It has been found that phase pure $BaTiO_3$ can be prepared at a temperature as low as 175^0C. The XRD patterns revealed the $BaTiO_3$ is well crystalline.

Figure 5.2 plots the average crystallite size as a function of calcination temperature. As expected, crystallite size increases with increasing calcination temperature. At low temperature calcined $BaTiO_3$ powder has lower crystallite size and found to be around 30 nm and it increases to 40 nm for 500^oC calcined sample. The lattice parameter determined from XRD using Unit Cell software and the c/a ratio found to be 1.0005. There is no significant variation of c/a ratio with calcinations temperature. This may be considered as pseudocubic structure. Begg et al. [2] had also reported that tetragonality increases with increase in crystallite size. The maximum tetragonality in $BaTiO_3$ single crystal was

observed 1.0095 [3].The tetragonality (c/a ratio) was found to increase with increase in calcination temperature.

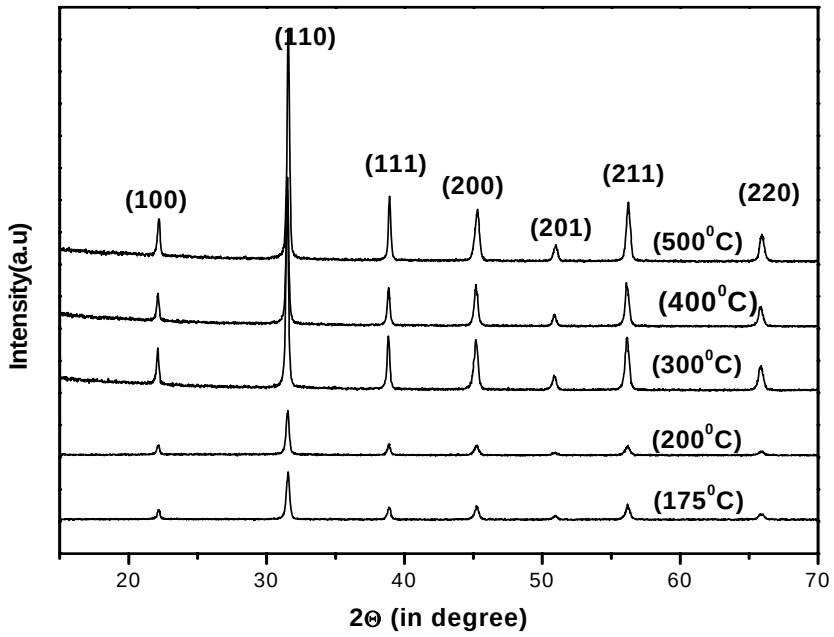

Fig 5.1 XRD pattern of $BaTiO_3$ Powder calcined at different temperature for 2h.

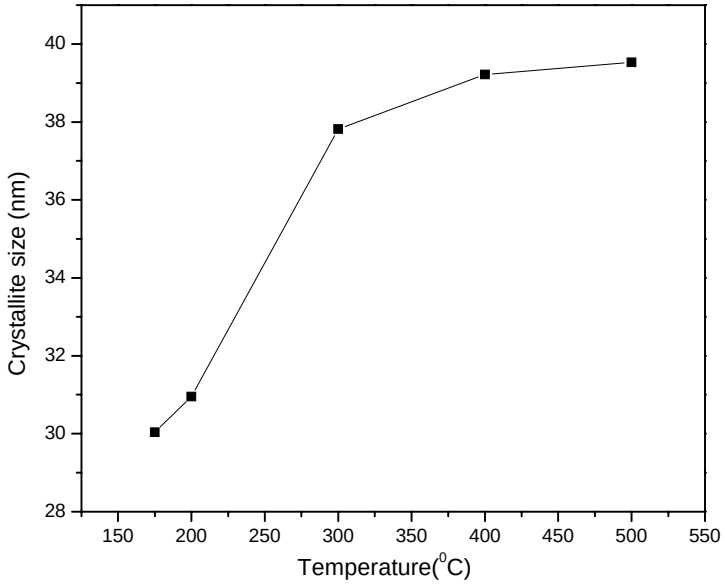

Fig 5.2 The average crystallite size of $BaTiO_3$ Powder calcined at different for 2h.

Fig 5.3 (XRD) shows the phase formation behavior of $BaTiO_3$ on dwelling time at a particular temperature. It has been found that the phase pure material can be found out in 30 min soaking time. Increase in dwelling time only increases the crystallite size.

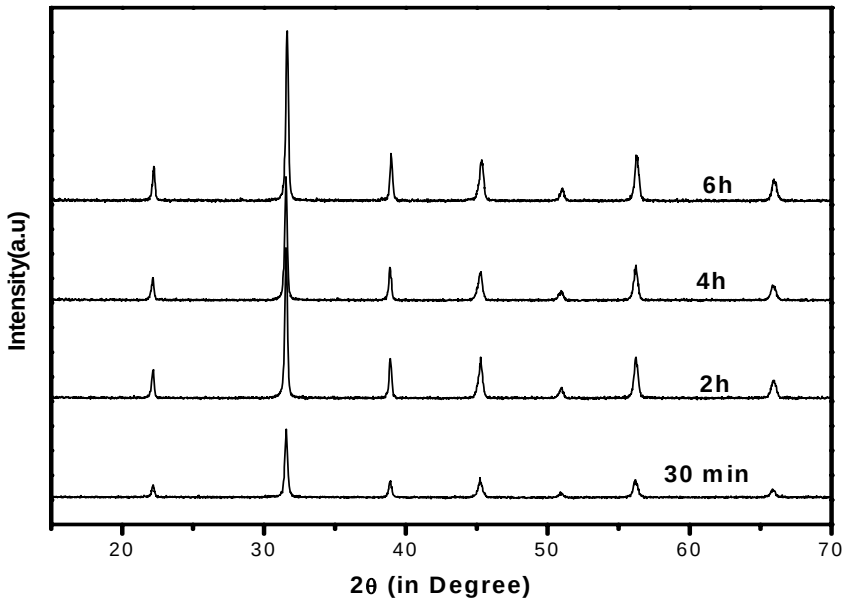

Fig 5.3 XRD pattern of $BaTiO_3$ Powder calcined at 300^0C with different soaking period.

The effect of using a hydroxide salt can be summarized as follows. It turns out that the hydroxide ion can actively participate in the reaction itself. For instance, it has been shown that molten hydroxide solutions [4] will not only react with metallic salts but also with metal oxides present. A plausible formation mechanism for $BaTiO_3$ is given in the presence of NaOH as the salt medium. KOH yields soluble K_2CO_3 as a byproduct, but otherwise the analysis is exactly the same as with NaOH alone.

$$BaCO_3 + 2NaOH + TiO_2 \longrightarrow BaTiO_3 + Na_2CO_3 + H_2O$$

In the absence of hydroxide ion a correspondingly viable reaction is simple solid state reaction :

$$BaCO_3 + TiO_2 \longrightarrow BaTiO_3$$

Probably the large apparent difference in free energy of reaction coupled with the relatively high solubility and reactivity of metal species in hydroxide media can therefore explain the relative ease and overall completeness of $BaZrO_3$ formation that we have observed [5].

(B) **NaCl-KCl salt system**

Fig 5.4 shows the XRD Pattern of $BaTiO_3$ Powder synthesized by using NaCl-KCl eutectic salt mixture after calcination at the temperature ranging from 700-800^{0}C for 2h. In this salt system the eutectic temperature is 658^{0}C. The phase pure of $BaTiO_3$ can be prepared at700^{0}C for 2h which is lower than the earlier report [6]. The crystal structure is pseudocubic in nature with a c/a ratio 1.0005. In these salt system has found to higher tetragonality than that of previous salt system. The Average crystallite size calculated using Scherer's formula [7] was found to be 35 nm when the powder calcined at 700^{0}C. It was found that with increasing calcination temperature the crystallite size increases. The crystallite size was found to be 35 nm for lowest calcination temperature 700^{0}C for 2h and it was 37 nm for highest calcination temperature 800^{0}C for 2h.

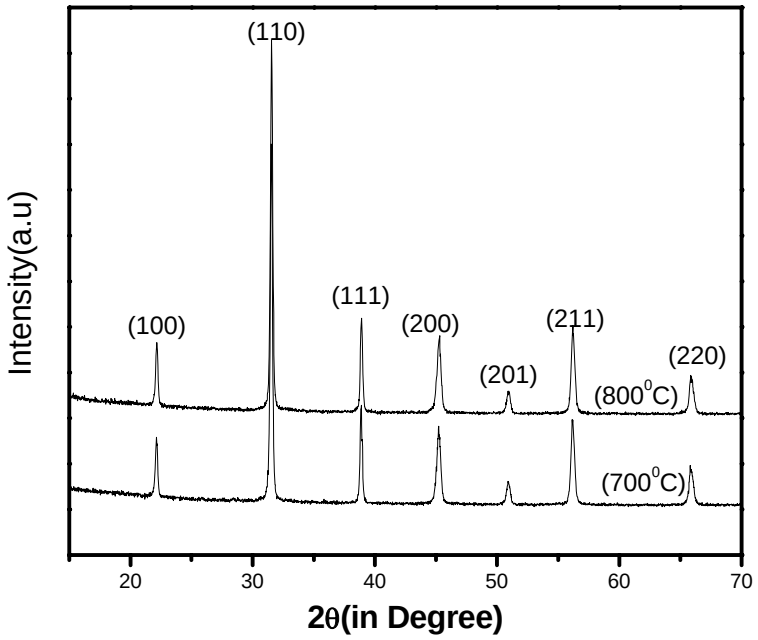

Fig 5.4 XRD pattern of $BaTiO_3$ calcined Powder at different temperature for 2h

Fig.5.5 shows the XRD pattern of the $BaTiO_3$ powders calcined at 700^{0}C for different Soaking Period. It is clear from the pattern that 30 min heat treated sample contains impurity phase $BaTi_2O_5$. But in NaOH-KOH system has no impurities phase found in the 30 min soaking period. It was found that the crystal structure does not change with the increase in the soaking period only crystallite size changes with increase in soaking period.

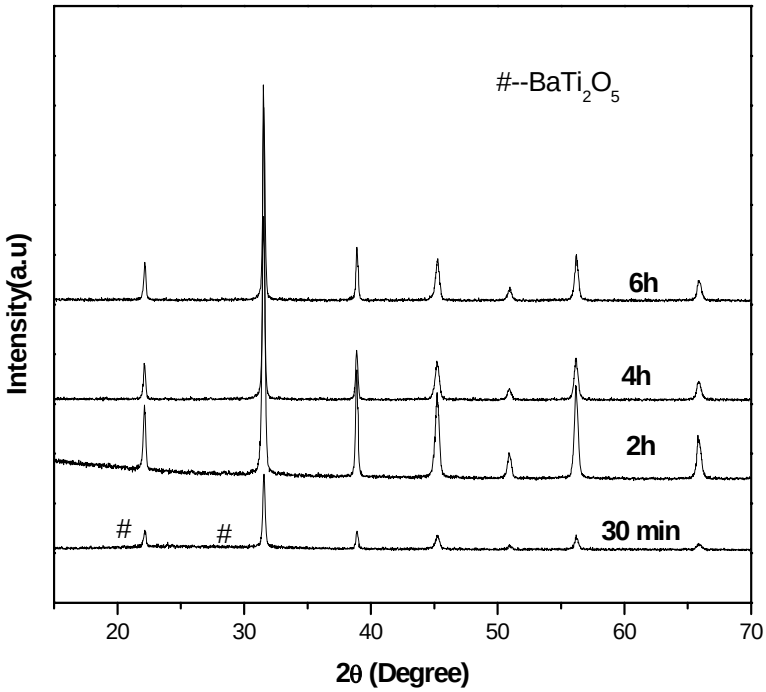

Fig 5.5 XRD pattern of $BaTiO_3$ calcined Powder at 700^0C with variation of soaking periods

In solid state mixing method at least 800^oC is required for getting phase pure $BaTiO_3$. By contrast, in the salt system phase pure powder formed at 700^oC. The possible reason may be, in the presence of NaCl-KCl, precursor molecules will more readily disperse, dissociate, rearrange, and then diffuse rapidly throughout the salt, forming a reasonably homogeneous solution that fosters rapid reaction. Higher temperatures therefore not only increase the flux and mobility of reactive components but also imply a lower viscosity within the reaction medium, all of which is consistent with a higher rate of reactivity [8] .

(C) LiCl-KCl salt system

Although KCl-LiCl salts have a low melting temperature of 358^0C, it is interesting to note that the perovskite phase was not formed till at 500^oC shown in fig 5.6. Unreacted $BaCO_3$ and TiO_2 Phases were found. The salt system was rejected to prepare the perovskite phase.

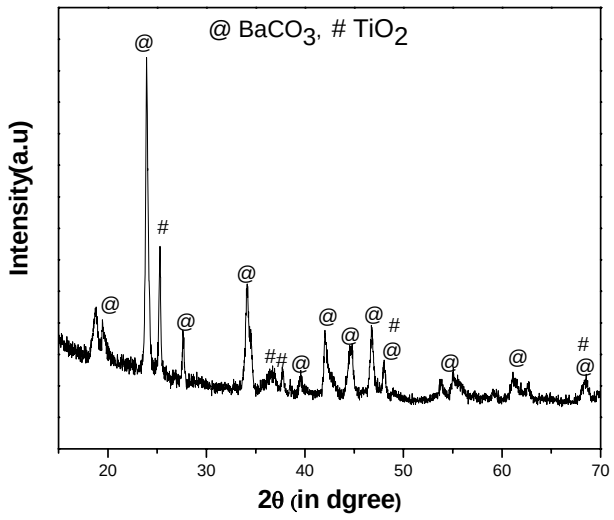

Fig 5.6 XRD pattern of $BaTiO_3$ calcined Powder at 500^0C using KCl-LiCl salt system at 2h

5.3 Particle size Analysis

(A) **NaOH-KOH salt system**

The particle size distribution was measured by ZETA Sizers Nanoseries. The particle size distribution were carried of different Calcined temperature of $BaTiO_3$ are shown in fig 5.7. The Particle Size were found to be in the range of 125-250nm. The observed particle size are basically represents the agglomerate size formed during the calcination. From the graph the particle size were increases with increase in calcination temperature. However, the X-ray study suggests that the particle will be in the nanometer. The difference between the results may be reconciled by assuming that the fine nanometer range particles get agglomerated during the heat treatment and washing. The agglomerate formation may result from the fineness of the powder, which was supposed to have high surface energy. The high surface energy of the powder leads to the development of the agglomerate during washing. The particles size was also depend upon the both calcination temperature and soaking period. Variations of soaking period changes the particles size were observered in fig 5.8.The average particle size were found to be in the range of 125-300nm.

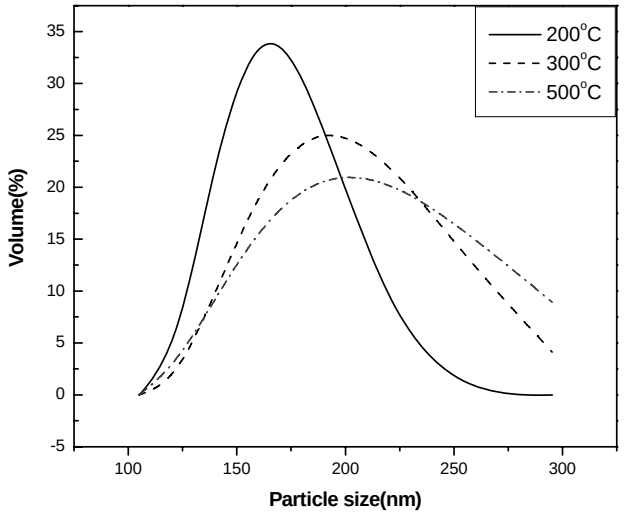

Fig 5.7 Particle Size of $BaTiO_3$ powder calcined at different temperature for 2h.

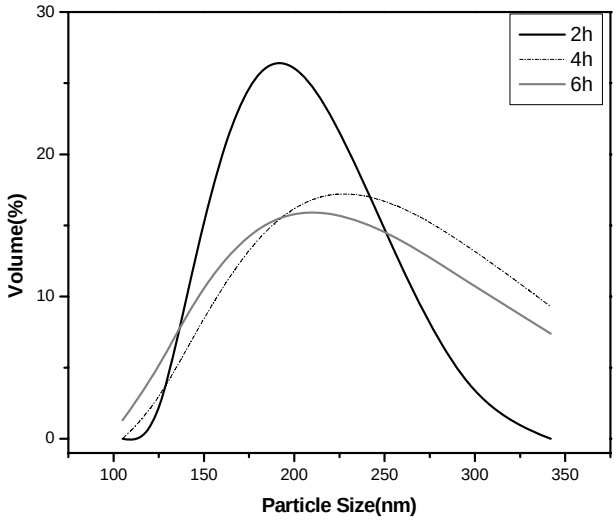

Fig 5.8 Particle Size of $BaTiO_3$ Powder calcined at 300^0C using salt NaOH-KOH system with variation of Soaking period

(B) **NaCl-KCl salt system**

Fig.5.9 shows the particle size distribution of $BaTiO_3$ powder calcined at different temperature ranging from 700-800^0C for 2h. The average particles size was found to be in the range of 150-350nm. Increase in heat treatment temperature gives higher and broad particle size distribution. The particle size distribution was also depends upon the reaction time. The

time variation of $BaTiO_3$ calcined powder was shown in fig 5.10. The graph clearly shows the increase in the particle size with respect to time.

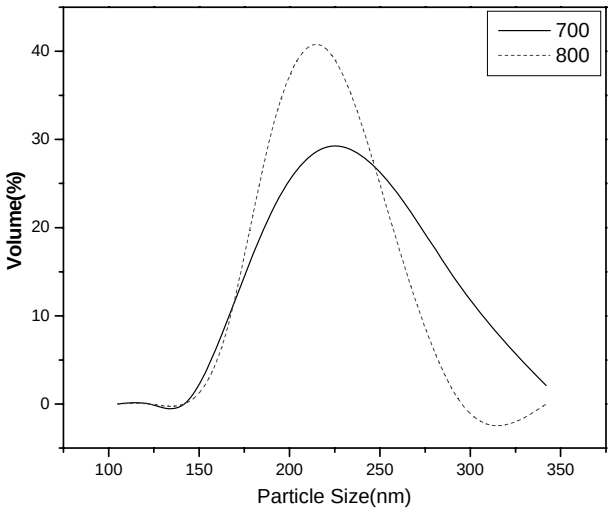

Fig 5.9 Particle Size of $BaTiO_3$ calcined Powder at different temperature for 2h.

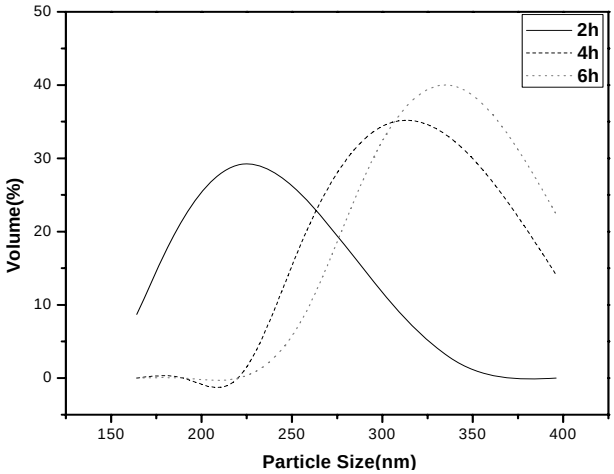

Fig 5.10 Particle Size of $BaTiO_3$ Powder calcined at 700^0C with variation of Soaking period.

5.4 Powder Morphology Analysis

(A) NaOH-KOH system

Figure 5.11 shows the SEM morphology of the synthesized powders prepared at 200^0C-500^0C for 2 h. The powders obtained contain a large portion of agglomerates with a small particulate size. Since the agglomeration was sufficiently small and soft, there was no need for a milling process. It could be clearly observed that the agglomerates are actually formed

from very small particle in naometric range size. Although the agglomerates are of irregular size the fine naometric particles are mostly cubic in size and some spherical particles are there. EDX analysis of the particles failed to give any Na, K content.

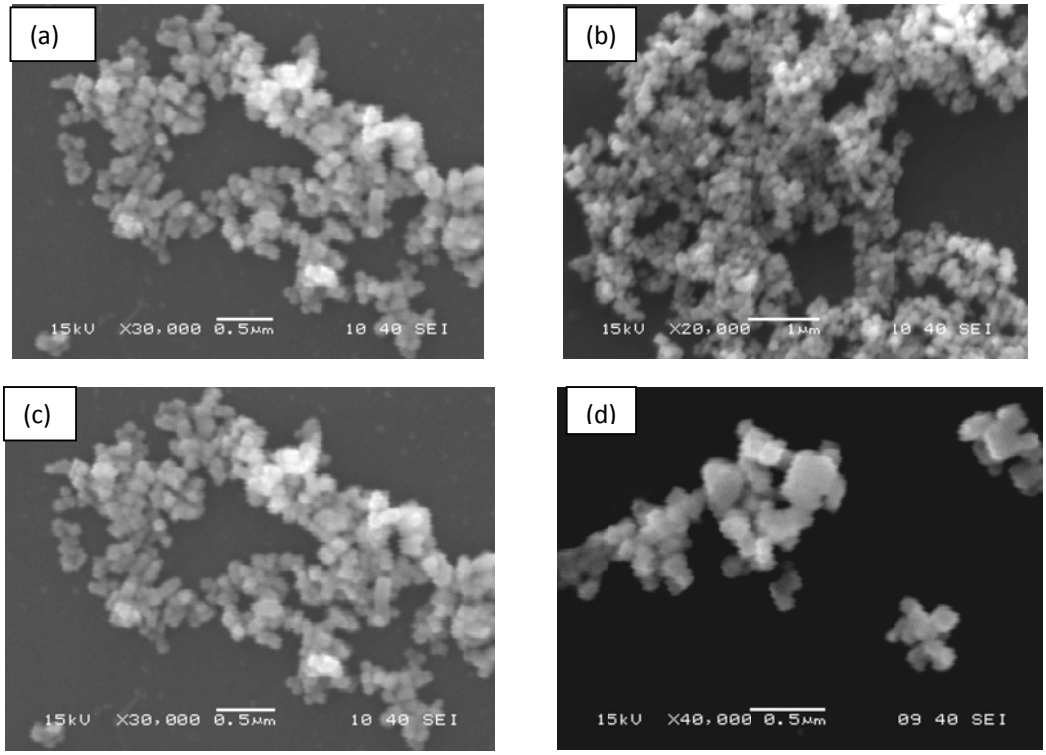

Fig 5.11 Microstructure of $BaTiO_3$ powder calcined at different temperature for 2h (a) 200^0C (b)300^0C (c)400^0C (d) 500^0C

(B) NaCl-KCl system

In the salt system, the SEM morphology of the synthesized $BaTiO_3$ powders prepared at temperature 700^0C for 2 and 6h. The effect of dwell time on the morphology of the calcined powders was also found to be quite significant. It is clearly seen that longer heat treatment led to larger particles and hard agglomeration. The particle size found to be in the range of 200-500nm for 6h sample and the agglomerates are of irregular in shape.

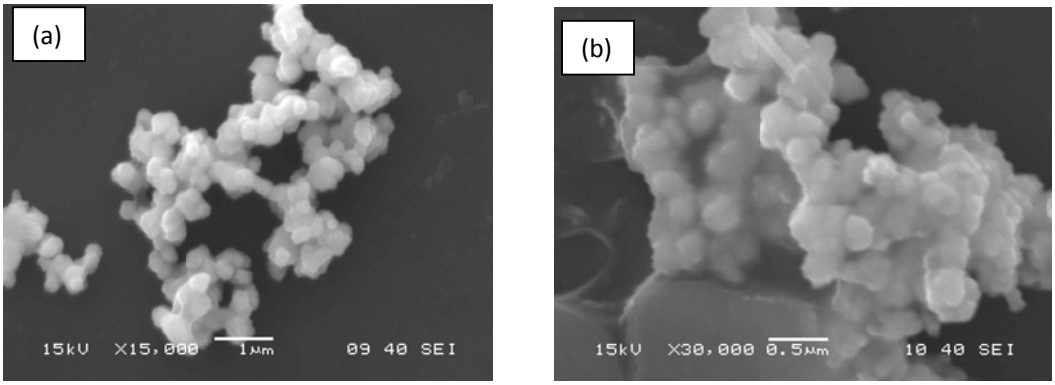

Fig 5.12 Microstructure of $BaTiO_3$ powder calcined at 700^0C at different time (a) 2h (b) 6h

From SEM study it is very difficult to find out the exact morphology of the individual particle. So TEM analysis was done for two samples.

5.5 TEM analysis of $BaTiO_3$ Powder

The TEM images of the prepared $BaTiO_3$ powders for different salt system is shown in Fig 5.13 The TEM image shows that the average size of $BaTiO_3$ is about 70-90 nm with cubic shape in case of NaOH-KOH salt system and for NaCl-KCl salt system similar cube shape with some spherical particle present.

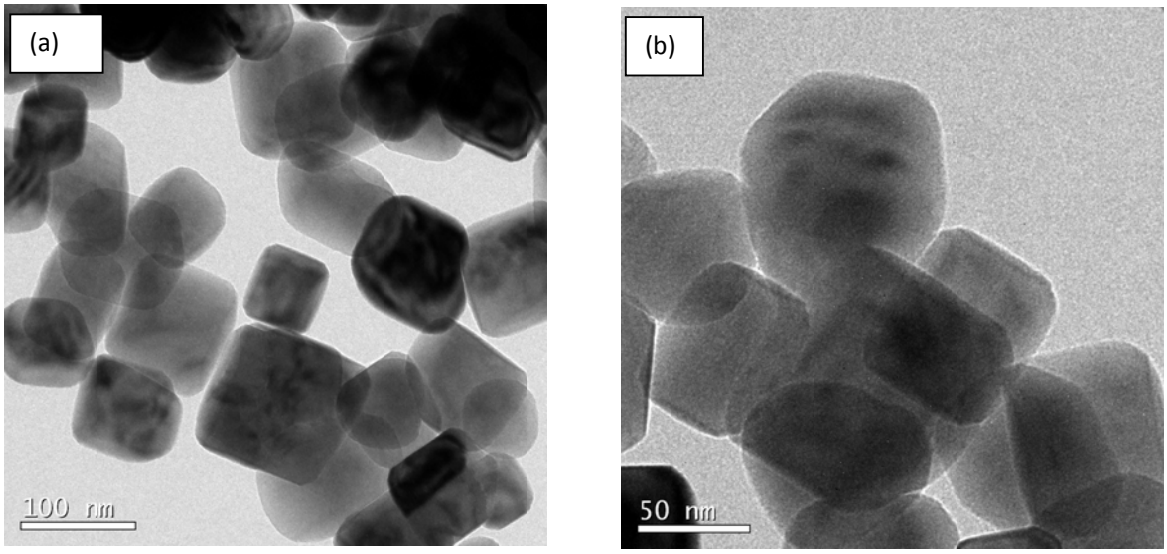

Fig 5.13 TEM micrograph of $BaTiO_3$ powder prepared by using NaOH-KOH salt system (a) 500^oC calcined (b) 700^oC calcined (NaCl-KCl salt system)

5.6 XRD analysis of sintered $BaTiO_3$ sample

(A) NaOH-KOH system

Finally the powder compact was sintered at 1225^{o}C for 3 h. The Fig 5.14shows the XRD pattern of sintered and ground pellets which were prepared using powders calcined different temperature (200-400^{o}C). It is clear that the low calcination temperature prepared $BaTiO_3$ sample produces impurity mainly $BaTi_2O_5$.The impurity phase disappears when the calcination temperature of powder increases above 300^{0}C. Fig 5.15 is the closer observation on the (002) and (200) planes of the X-ray diffractogram of calcined and sintered $BaTiO_3$ sample. The figure shows the splitting of peaks only initiate in the sintered sample. This may be due to the crystal structure change of $BaTiO_3$ from metastable cubic to tetragonal [2].

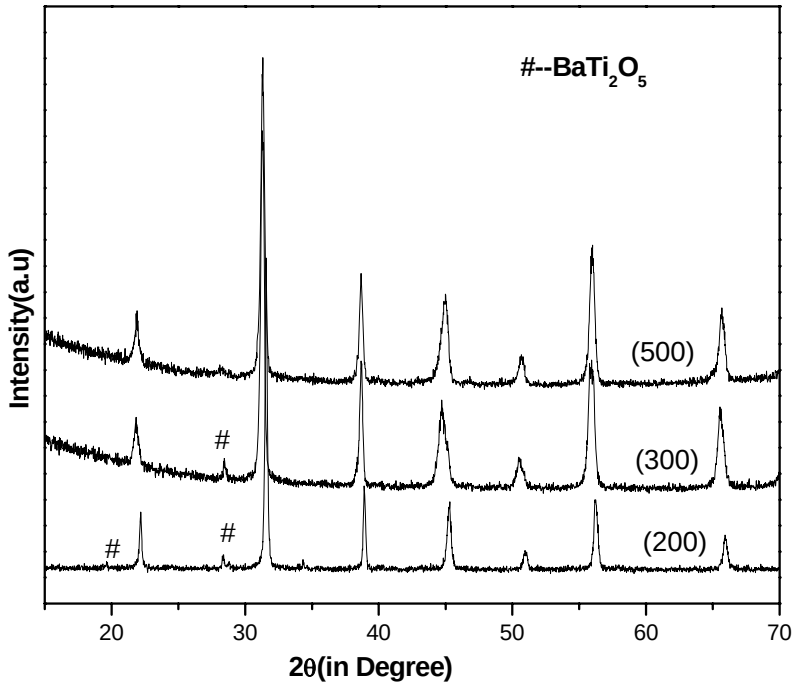

Fig 5.14 XRD pattern of different calcination temperature $BaTiO_3$ sample Sintered at 1225^{0}C for 3h

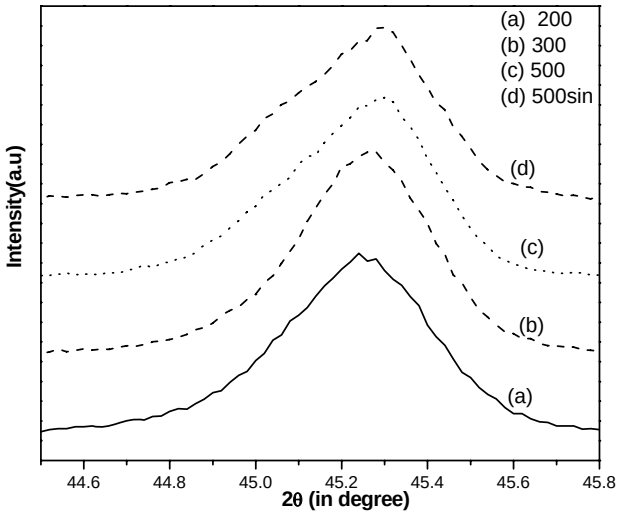

Fig 5.15 XRD patterns showing the splitting of (200) and (002) peaks of $BaTiO_3$ as a function of temperature

(B)NaCl-KCl system

Fig 5.16 shows the XRD pattern of sinter $BaTiO_3$ sample. Phase purity was retained in sintered sample and no secondary phase can be found.

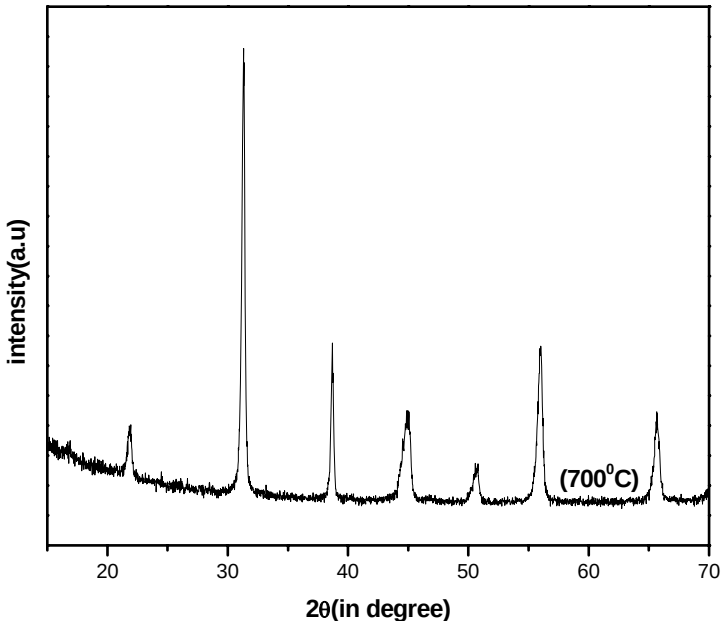

Fig 5.16 XRD pattern of $BaTiO_3$ sample Sintering at 1225^0C for 3h

For further studies e.g. Density measurement, electrical characterization impurity free sintered samples are taken.

5.7 Density of sample

The relative density of sintered sample prepared by using NaOH-KOH salt system powder at 1225^0C for 3h has been found to be more than 97% of theoretical density. But at same temperature NaCl -KCl based powder gives only 91% of theoretical density. Further enhancement of sintering temperature produces deformation of the sintered sample. Further studies are required to understand the sintering behavior of these ultrafine powders.

5.8 Microstructure of Sintered sample

(A) NaOH-KOH system

The SEM micrographs of the polished and thermal etched section of $BaTiO_3$ of different temperature calcined samples sintered at 1225^0C for 3 hour have been shown in Fig. 5.17 (a) and (b)**.** The microstructure reveals that highly dense structure with small grain size. Interestingly, fine grain size (0.2-0.5 μm) was retained in highly dense sintered sample.

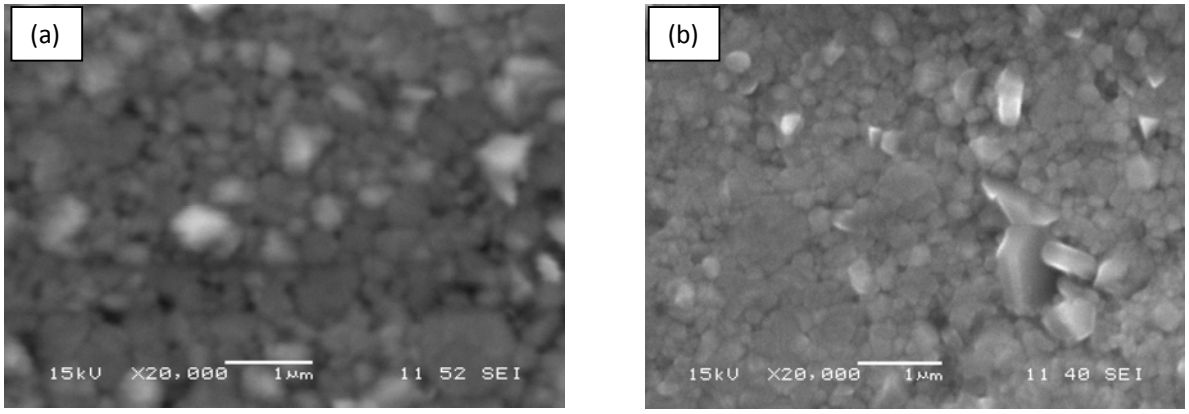

Fig 5.17 Microstructure of sintered $BaTiO_3$ sample sintered at 1225^0C for 3h for different calcination temperature (a) 300^0C (b) 500^0C

(B) NaCl-KCl system

NaCl-KCl based sintered sample shows significant amount of porosity which corroborate the low sintered density of the sample. The porosity present in the samples are intergranular in nature, the intragranular pores are not observed. Form the microstructure it is very difficult to identify the grain size. It seems that small grains are fused and formed large mass.

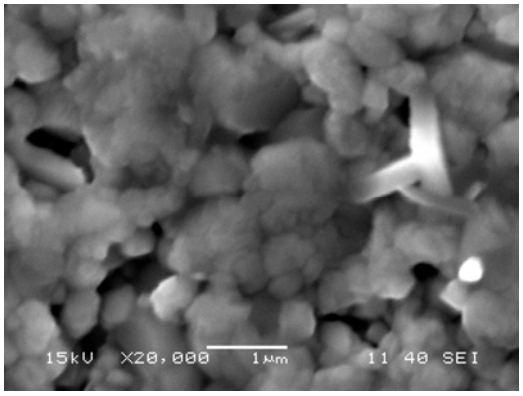

Fig 5.18 Microstructure of sintered $BaTiO_3$ sample sinter 1225^0C for 3h

5.9 Dielectric Properties of $BaTiO_3$ sample

5.9.1 Room temperature dielectric behaviour of $BaTiO_3$

(A). NaOH-KOH system

Fig 5.19 shows the dependence of relative permittivity and dissipation factor with frequency. Samples show small frequency dispersion. The relative permittivity and tanδ value found to be 1400 and 2% at 1kHz respectively which are on a par with $BaTiO_3$ prepared via conventional method. Recently wada et. al. reported a relative permittivity of 5000 for 140 nm grain size sample [9]. But in our case value is less that may be due to the lack of prominent tetragonality in the sintered sample.

Fig.5.19 Variation of dielectric constant and loss tangent of sintered $BaTiO_3$ pellets with frequency for NaOH-KOH salt system prepared powder

(B) NaCl-KCl system

NaCl-KCl based sample shows higher dielectric constant with higher loss compared to NaOH-KOH based sample. The high dielectric loss in the sintered sample is due to the porosity effect as it decreases with the increase in frequency.

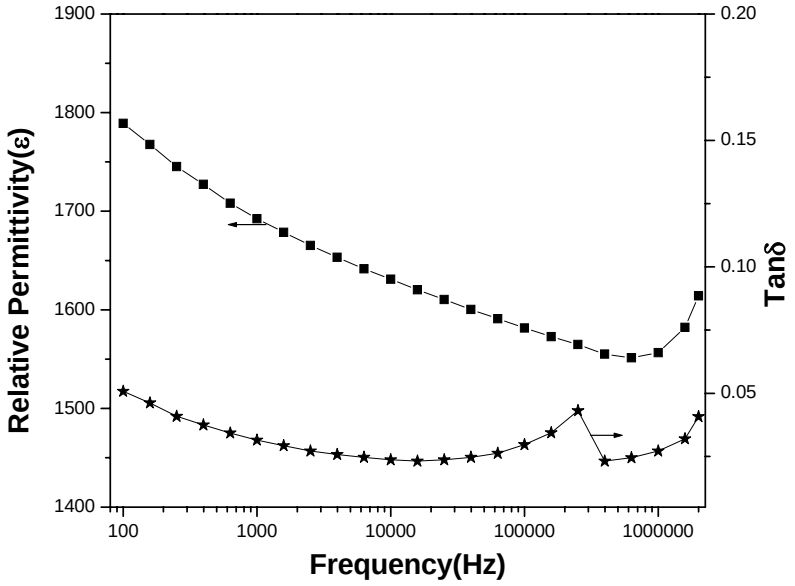

Fig.5.20 Variation of dielectric constant and loss tangent of sintered $BaTiO_3$ pellets with frequency for NaCl-KCl salt system prepared powder

5.9.2 Temperature dependent dielectric behaviour of $BaTiO_3$

(A) NaOH-KOH system

Fig.5.21 (a) shows the variation of relative permittivity of $BaTiO_3$ samples with temperature for different frequencies. It is clear from the figure that the conventional-sintered $BaTiO_3$ materials possess high relative permittivity (ε_r = 1500) at room temperature with very flat relative permittivity–temperature (ε_r–T) properties. The peak at the Curie temperature of $BaTiO_3$ materials is completely suppressed. Probably small grain size transforms the crystal structure towards the cubic symmetry [10].

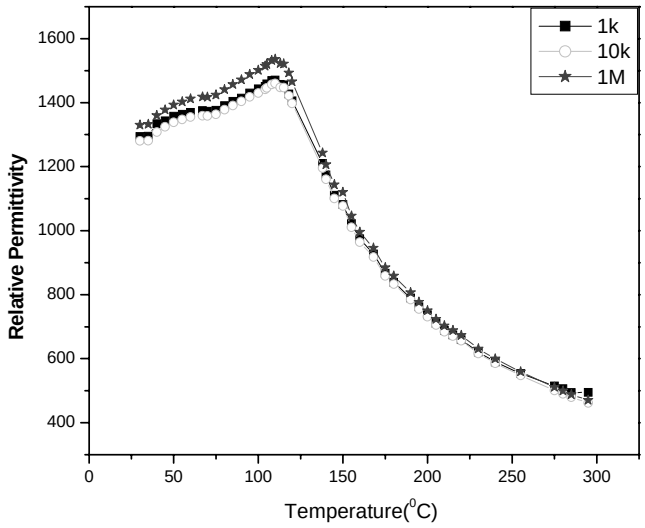

Fig 5.21 (a) Temperature dependent relative permittivity of $BaTiO_3$ ceramics sintered at 1225^0C

Incidentally, the rise of DF (Fig. 5.20 (b)) with temperature indicates the thermally activated nature (increase ac conductivity with frequency) of dissipation.

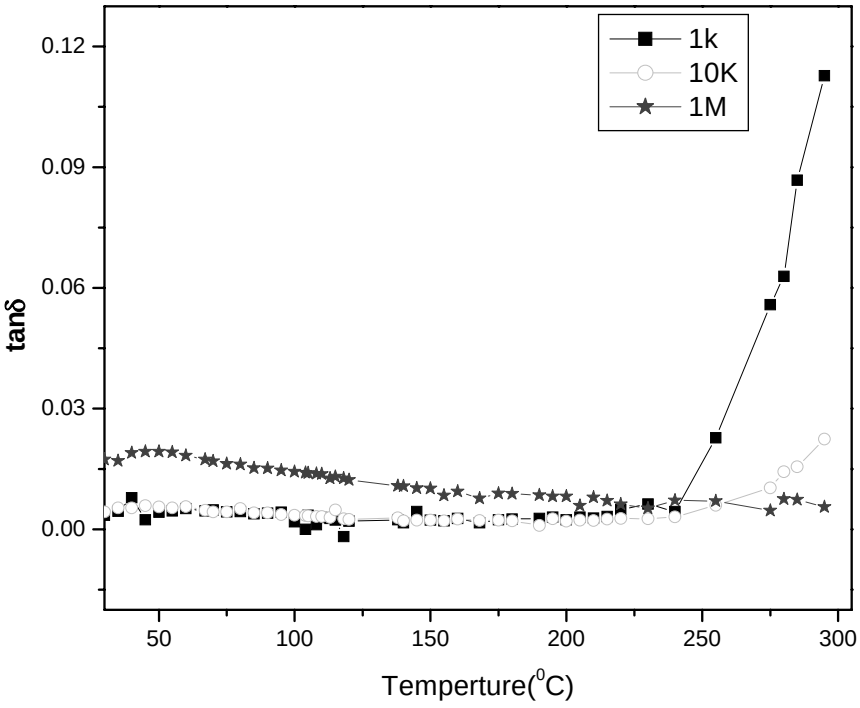

Fig 5.21(b) Temperature dependent dissipation factor (tanδ) of $BaTiO_3$ceramics sintered at 1225^0C

(B) NaCl-KCl system

Fig 5.22 shows dependence of the relative permittivity with temperature. It shows a broad peak around Curie temperature, the peak height decreases with the increase in frequency and the peak top (T_{max}) was shifted to lower temperature. It can be explained from a 3-layer model, including surface cubic layer, bulk tetragonal layer, and gradient-lattice-strain layer (GLSL) between surface and bulk layers [11] of the grain. The GLSL has very high dielectric constants because of low tetragonality just below the T_c. Therefore, for temperature dependence of dielectric constants in the GLSL, a summation of different T_{max} below Curie temperature can result in a formation of broadening dielectric peak with lower T_{max} than T_c.

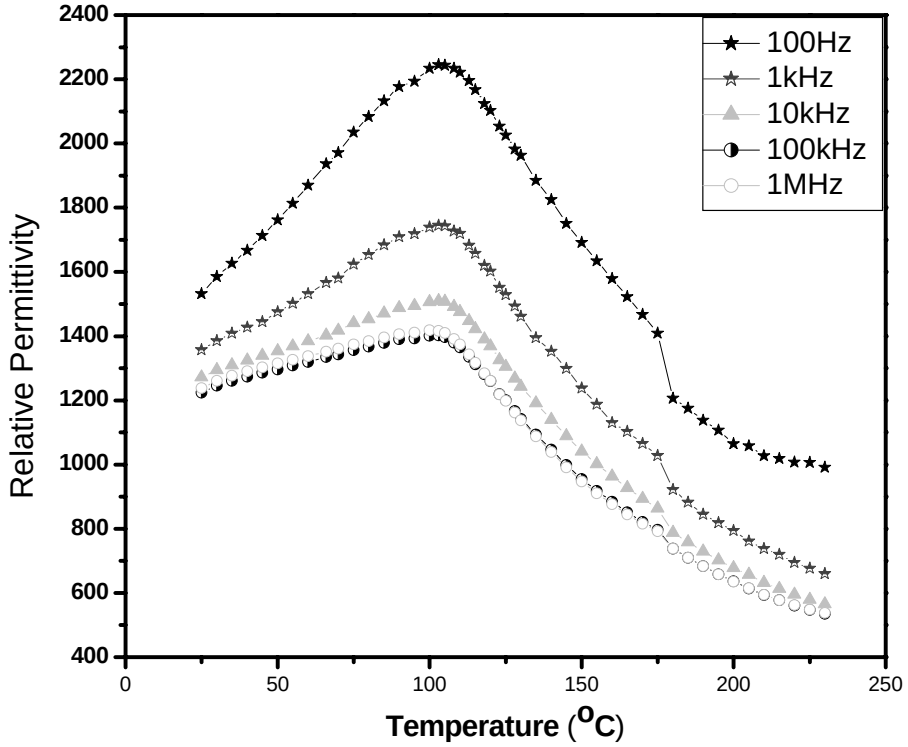

Fig 5.22 Temperature dependent relative permittivity of $BaTiO_3$ ceramics sintered at 1225^0C

5.10 P-E loop analysis

Fig. 5.23 shows the P–E loops of the $BaTiO_3$ sample prepared by NaOH-KOH based system. Measurement field was beyond the saturation limit. The remanent polarization value was less than the literature reported value. That can be attributed to smaller grain size and lack of tetragonality in the sintered sample.

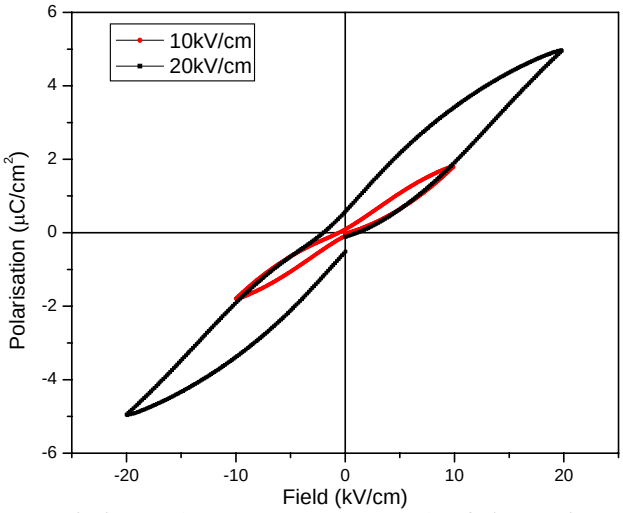

Fig 5.23 P–E hysteresis loops (at room temperature) of sintered $BaTiO_3$ sample under varying electric field of NaOH-KOH salt based system.

References

1. Gopalan Srikanth, Mehta Karun, and Virkar Anil V. Journal of materials research 11:88, 1863-1865,

2. Begg, Bruce D., Vance, Eric R., Nowotny, Janusz (1994) Journal of the American Ceramic Society*, 77* (12), pp. 3186-3192.

3. Lin, S., Lu, T., Jin, C., Wang, X. Physical Review B - Condensed Matter and Materials Physics 74 (13), art. no. 134115 (2006)
4. Liu, H.; Hu, C.; Wang, Z. L. *Nano Lett.* 2006, *6*, 1535.
5. Hongjun Zhou, Yuanbing Mao, and Stanislaus S. Wong, *Chem. Mater.* 2007, *19,* 5238-5249

6. Yuanbing Mao,Sarbajit Banerjee, and Stanislaus S. Wong J. Am. Chem. soc. 2003, 125, 15718-15719
7. Wada. S., Hoshina. T, Yasuno H., Ohishi, M., Kakemoto, H., Tsurumi, T., Yashima. M Ceramic Transactions 174, pp. 15-26 (2006)
8. Bloom, H. *The Chemistry of Molten Salts*;W. A. Benjamin, Inc.: New York, 1967.
9. Wada Satoshi, Yazawa Aki, Hoshina Takuya, Kameshima Yoshikazu, Kakemoto Hirofumi, Tsurumi Takaaki, and Kuroiwa Yoshihiro IEEE Transactions on Ultrasonics , Ferroelectrics , and Frequency Control , vol. 55, no. 9, September2008
10. Frey M. H. and Payne D. A. Phys. Rev. B, 54(5), 3158-3168 (1996)
11. T. Hoshina, H. Kakemoto, T. Tsurumi, S. Wada, M. Yashima, K.Kato, and M. Takata, *Key Eng. Mater.*, vol. 301, pp. 239–242, 2005.

Chapter 6

CONCLUSION

Conclusions

On the basis of the Molten Salt Synthesis of $BaTiO_3$ nano-sized particles, the effects of different parameters, such as salt system, reaction temperature, reaction time, on the resultant product purity, size, shape, and morphology have been discussed. Among these various parameters, the selection of salt is likely the most important one because solubility and reactivity effects associated with the salt can very significantly alter the synthesis process as well as the resultant particle size and shape. The densification behavior, microstructure and dielectric behavior of the sintered specimen were studied. The following conclusions can be obtained from this study.

Nanosized phase pure $BaTiO_3$ powder can be synthesized at a temperature as low as 175^{o}C by using the NaOH-KOH eutectic mixture. Crystallite size increases with increasing reaction temperature and time. Reaction temperature varied from 175-500^{o}C. TEM micrograph depict cube shaped particle with 70-100 nm size. NaCl-KCl based system produce phase pure powder at 700^{o}C with a pseudocubic symmetry. This system produce cube shaped with some fraction of round shaped particle. Where LiCl-KCl based system failed to produce phase pure powder.

Though NaOH-KOH based system produce phase pure powder at low temperature but it generates impurity phase when sintered at high temperature. For getting phase purity at the sintered product reaction temperature has to be increased to more than 300^{o}C. Tetragonality revealed in the sintered sample. This powder can be densified at 1225^{o}C with a sintered density more than 97%. Interestingly, the submicron sized (0.2-0.5 μm) grain retained in the sintered sample. It is very difficult to densify NaCl-KCl based synthesized powder more than 91% of the theoretical density.

Dielectric constant and loss factor of the (NaOH-KOH based) sintered samples (ε_r =1400 and tanδ = 2% at 1kHz) are on a par with the $BaTiO_3$ prepared via conventional solid state method where very high calcinations and sintering temperature is required. NaCl-KCl based sample shows higher dielectric constant with higher loss compared to NaOH-KOH based sample.

NaOH-KOH salt based prepared sample showed almost flatten Curie peak and NaCl-KCl salt system prepared sample showed broad Curie peak The peak shift and broadening can be explained qualitatively from temperature dependence of volume fraction between surface cubic layer, bulk tetragonal layer, and gradient-lattice-strain layer (GLSL)..